BARRA v1.0: The Bureau of Meteorology Atmospheric high-resolution Regional Reanalysis for Australia

Chun-Hsu Su[1], Nathan Eizenberg[1], Peter Steinle[1], Dörte Jakob[1], Paul Fox-Hughes[2], Christopher J. White[3,4], Susan Rennie[1], Charmaine Franklin[1], Imtiaz Dharssi[1], Hongyan Zhu[1]

[1] Bureau of Meteorology, Docklands, Victoria 3008, Australia
[2] Bureau of Meteorology, Hobart, Tasmania 7000, Australia
[3] Department of Civil and Environmental Engineering, University of Strathclyde, Glasgow, Scotland, UK
[4] Antarctic Climate and Ecosystems Cooperative Research Centre, Hobart, Australia

Correspondence to: C.-H. Su (chunhsu.su@bom.gov.au)

Abstract. The Bureau of Meteorology Atmospheric high-resolution Regional Reanalysis for Australia (BARRA) is the first atmospheric regional reanalysis over a large region covering Australia, New Zealand and southeast Asia. The production of the reanalysis with approximately 12 km lateral resolution – BARRA-R – is well underway with completion expected in 2019. This paper describes the numerical weather forecast model, the data assimilation methods, and the forcing and observational data used to produce BARRA-R, and analyses results from the 2003~~7~~-2016 reanalysis. BARRA-R provides a realistic depiction of the meteorology at and near the surface over land as diagnosed by temperature, wind speed, surface pressure, and precipitation. ~~It shows closer agreement with point-scale observations and gridded analysis of observations, than leading global reanalyses~~Comparing against global reanalyses ERA-Interim and MERRA-2,~~.~~ ~~In particular, BARRA-R improves upon ERA-Interim global reanalysis in several areas at point-scale to 25 km resolution.~~ BARRA-R ~~shows~~ scores lower root-mean-square errors when evaluated against (point-scale) 2 m temperature, 10 m wind speed and surface pressure observations. It also shows ~~reduced negative biases in (point-scale) 10 m wind speed during strong wind periods,~~ reduced biases in ~~(5 km gridded)~~ daily 2 m temperature maximum and minimum at 5 km resolution, and a higher frequency of very heavy precipitation days at 5 ~~km~~ and 25 km resolution when compared to gridded satellite and gauge analyses. ~~Few~~ Some issues with BARRA-R are also identified:~~;~~ ~~some of which are common in reanalyses, such as~~ biases in 10 m wind, lower precipitation than observed over the tropical oceans, higher precipitation over regions with higher elevations in south Asia and New Zealand. ~~and others that are more specific to BARRA such as grid point storms.~~ Some of these issues could be improved through dynamical downscaling of BARRA-R fields using convective-scale (< 2 km) models.

1 Introduction

Reanalyses are widely used for climate monitoring and studying climate change as they provide long-term spatially complete records of the atmosphere~~ for long periods that are a balance between physical consistency and observations~~. This is achieved by using data assimilation techniques that produce an observation-constrained model estimate of the atmosphere. They~~,~~ ~~by~~ draw~~ing~~ short-term model states towards observations from multiple, disparate sources to form an atmospheric analysis. ~~The use of a~~A physically realistic model ~~-~~provides the means to infer atmospheric states at locations without observations ~~enables the estimation of unobserved parameters~~ from the limited ~~and irregularly distributed~~ collection of irregularly distributed ~~observed parameters~~observations.

Global-scale reanalyses using global atmospheric circulation models (GCMs) have advanced in quality and quantity during the past two decades (Dee et al., 2014; Hartmann et al., 2013). At present, the available global reanalyses established for the satellite era include the NCEP/NCAR reanalysis at 210 km horizontal resolution (Kalnay et al., 1996), the Japanese 55-year Reanalysis (JRA-55) at 60 km (Ebita et al., 2011), the Modern-Era Retrospective analysis for Research and Applications-2 (MERRA-2) at about 50 km (Gelaro et al., 2017) and the European Centre for Medium Range Weather Forecasts (ECMWF) ReAnalysis Interim (ERA-Interim) at ~79 km (Dee et al., 2011). The latter is currently~~will be~~ being replaced by the new ERA-5 ~31 km reanalysis (Hersbach and Dee, 2016). These global reanalyses have the advantage~~s~~ of providing globally consistent information~~ and homogeneous reanalyses~~, but at the expense of spatial resolution. With resolutions typically greater than 50 km, they may be deficient in~~to~~ ~~cannot~~ accounting for important subgrid variations in meteorology over heterogeneous terrains and islands, and across irregular coastlines, and other small-scale processes (Mesinger et al., 2006; Randall et al., 2007, and references therein).

To address these shortcomings, the development in global reanalysis has also driven concurrent efforts in statistical approaches and dynamical downscaling (e.g., Dickinson et al., 1989; Fowler et al., 2007; Evans and McCabe, 2013). The latter typically embeds a high-resolution meteorological ~~or regional~~ ~~atmospheric~~ model within a global reanalysis, where effects of small-scale forcing and processes such as convection are modelled. Such development is supported by improvements in non-hydrostatic models that run at high resolution in operational numerical weather prediction (NWP) (e.g., Clark et al., 2016). Regional reanalyses are emerging as a step further in this direction. ~~One of the earliest~~The first regional reanalysis~~es~~ was the North America Regional Reanalysis (NARR, Mesinger et al., 2006). ~~, and the m~~More recent examples include the Arctic System Reanalysis (ASR, Bromwich et al., 2018), ~~and reanalyses for Europe and~~ Indian Monsoon Data Assimilation and Analysis (IMDAA, Mahood et al., 2018) and Uncertainties in Ensembles of Regional Reanalyses (UERRA) in Europe (Borsche et al. (2015) and therein). In contrast to dynamically downscaled global reanalyses, observations are used in regional reanalyses in the same way as in the global ones to reduce model errors in high-resolution simulations (Bollmeyer et al., 2015). The resulting ~~observation-constrained~~ reanalyses are expected to have better representations of frequency distributions, extremes and actual space and time-dependent variability (particularly for near-ground variables). UERRA consists of ~~Four~~

four ~~such European~~ regional reanalyses were developed by the Swedish Meteorological and Hydrological Institute (SMHI), Météo France, Deutscher Wetterdienst (DWD), and UK Met Office (UKMO)~~ within the (recently concluded) European (EU) Seventh Framework Programme (FP7) Uncertainties in Ensembles of Regional Reanalyses (UERRA) project (Borsche et al. (2015) and therein),~~ ~~. The project has~~ producing~~ed~~ an ensemble~~ range~~ of high resolution (5–25 km) ~~ensemble of~~ regional reanalyses of essential climate variables. ~~, and of which, t~~The SMHI's HARMONIE [Hi-Resolution Limited Area Model (HIRLAM) Aire Limitée Adaptation Dynamique Développement International (ALADIN) Regional/Mesoscale Operational NWP in Europe] reanalysis has ~~now~~ entered production for the Copernicus Climate Change Service (Ridal et al., 2017). ~~.~~

Regional reanalyses provide significant added value to their global counterparts in diverse applications ranging from traditional climate studies to industry applications, including regional climate change assessments that include local impact studies (e.g., Fall et al., 2010) and extreme events reconstruction (e.g., Zick and Matyas, 2015). As the regional reanalyses are generally produced with high spatial as well as temporal resolution, the extremes of variables at local scales ~~can~~may be quantified more accurately. They ~~can provide~~are also an alternative reference to evaluate climate projections (e.g., Ruiz-Barradas and Nigam, 2006; Radic and Clarke, 2011). At the same time, embedded forecast models can be used within the framework of the Coordinated Regional Climate Downscaling Experiment ~~(CORDEX)~~ (CORDEX, Martynov et al., 2013) within a seamless framework for weather and climate prediction, where model deficienc~~y~~ies~~ in the individual areas~~ that differ in spatial and time scales~~,~~ can be more readily understood (Brown et al., 2012)~~to produce seamless data, where similar modelling systems produce both historical data and projections to provide a higher level of consistency than otherwise possible~~. They also offer useful data sets for designing new infrastructure, particularly if they are sufficiently long and spatially relevant ~~in spatial resolution and extent~~ to define the likelihood of extremes. For renewable energy production, they can provide valuable information on ~~,~~ ~~and~~ intermittency (e.g., wind lull) and covariability (e.g., correlation spatially or between variables) of phenomena. For instance, COSMO (Consortium for Small-scale Modelling) 6 km reanalysis has shown the potential to provide realistic sub-daily representations of winds at 10 to 40 m height (Borsche et al., 2016), and to resolve small-scale cloud structures (Bollmeyer et al., 2015). NARR ~~has been~~was used to define a climatology of surface wind extremes (Malloy et al., 2015), and 30-year trends in wind at hub height (Holt and Wang, 2012) over northern America.

To date, while ~~the~~ regional reanalyses exist~~s~~ for~~in~~ North America, Europe and India, no atmospheric regional reanalysis for the Australasian region has been produced. To ~~address~~ close this gap, the Bureau of Meteorology Atmospheric high-resolution Regional Reanalysis for Australia (BARRA, Jakob et al., 2017) has been produced. BARRA is the first atmospheric regional reanalysis ~~for the Australasian region, with a domain~~that ~~covering~~ covers Australia, New Zealand, southeast Asia, and south to the Antarctic ice edge (Figure 11~~Figure 1~~). It is produced by the Australian Bureau of Meteorology (Bureau), with sponsorship from ~~in partnership with~~ state fire and governmental agencies across Australia, because of the important advantages it ~~allows~~ provides for planning and management to reduce risks due to extreme weather events including bushfires. For instance, BARRA will address the lack of accurate climate information on highly variable surface winds over large areas of Australia due to the low density of the surface observation network in remote areas ~~to sufficiently observe high variability in wind~~. BARRA covers a 29~~8~~-year period from 1990 to 2018~~7~~, with possible further extensions back and forward in time. The BARRA project delivers a whole-of-domain reanalysis (identified as BARRA-R) with approximately 12 km lateral resolution, and additional convective-scale (1.5 km horizontal grid-length) downscaling~~ed reanalyses~~ (BARRA-x), nested within BARRA-R, centred on major Australian cities to generate additional high-resolution information needed for local-scale applications and studies. ~~They produce a range of gridded data products over their respective domains at their respective resolutions.~~ These resulting gridded (12 km and 1.5 km) products include a variety of 10 min to hourly surface parameters, describing weather and land-surface conditions, and hourly upper-air parameters covering the troposphere and stratosphere. The fields on standard~~ized~~ pressure levels are generated from vertical interpolation of model-level fields. ~~These products include a variety of surface parameters, describing weather and land-surface conditions, at 10 minutes to hourly time resolution, and upper-air parameters on pressure and model levels covering the troposphere and stratosphere at hourly time resolution.~~ BARRA serves to lay the foundation for future generations of reanalyses at the Bureau and to further develop its capabilities to produce seamless climate information that integrates its observational networks and NWP programme.

In this paper, we describe the forecast model, data assimilation methods, and the forcing and observational data used to produce BARRA-R in Section 2. Section 3 provides an initial assessment of the reanalysis system over the first 14~~ten~~ years 20~~07~~03-2016, with a focus on analysing the quality at or near the surface; Section 4 concludes with a brief summary of our findings.

2 The BARRA-R reanalysis

The development of BARRA ~~follows~~ builds on~~from~~ the Bureau's experience in operational (deterministic) NWP forecasting over the Australian region using the Australian Community Climate and Earth-System Simulator (ACCESS)-R system (Bureau of Meteorology, 2010; 2013; Puri et al., 2013), and BARRA-R is produced using the UKMO's ~~UERRA~~ system in UERRA (based on Jermey and Renshaw, 2016) but without the ensemble component. An ensemble NWP forecast system is currently under development at the Bureau. BARRA-R is ~~belongs to a class of reanalyses~~ produced by running a limited-area meteorological forecast model forced with ~~a~~ global reanalysis' boundary conditions, ~~but~~ drawn closer to observations via data assimilation. ~~In other words, the forecast model provides the means to infer atmospheric states at locations without observations.~~ This section provides an overview of these components while more technical details are included in the references.

2.1 Forecast model

The Unified Model (UM, Davies et al., 2005) is the grid-point atmospheric model used in BARRA-R and ACCESS. It uses a non-hydrostatic, fully compressible, deep-atmosphere formulation and its dynamical core (Even Newer Dynamics for General atmospheric modelling of the environment, ENDGame) solves the equations of motion using mass-conserving semi-implicit, semi-Lagrangian time-integration methods (Wood et al., 2014). The model includes a comprehensive set of parametrizations, including a modified boundary layer scheme based on Lock et al. (2000), a variant of Wilson and Ballard (1999) for mixed-phase cloud microphysics, the~~a~~ mass flux convection scheme of Gregory and Rowntree (1990), and the radiation scheme of Edwards and Slingo (1996), which have all since been improved. ~~-~~Other~~The~~ parametrized sub-grid scale processes include ~~convection~~, ~~radiation,~~ fractional cloud cover ~~,~~ and ~~microphysics,~~ orographic drag ~~and boundary layer turbulence~~. More details on all of the physics schemes can be found in Walters et al. (2017a).

The prognostic variables are three-dimensional wind components, virtual dry potential temperature and Exner pressure, dry density, and mixing ratios of moist quantities. ~~The grid discretization~~The model is discretized on ~~uses~~ a horizontally staggered Arakawa C-grid (Arakawa and Lamb, 1977) and a vertically staggered Charney-Phillips grid (Charney and Phillips, 1953). The staggered arrangement of grid points allows for accurate finite differencing but results in different model fields located on staggered grids displaced by half a grid spacing along both axes. Data has been left on the staggered grids to allow users to apply the most appropriate re-gridding methods suited for given applications. The vertical levels smoothly transition from terrain-following coordinates near the surface, to constant height surfaces in the upper atmosphere (Davies et al., 2005).

BARRA-R uses version 10.2 of the UM and is configured with 70 vertical levels extending from near the surface to 80 km above sea level: 50 model levels below 18 km, and 20 levels above this. While configured with this height based on ACCESS-R, we have more confidence in the data up to a height of 25-30 km where we have most information from observations. The horizontal domain of BARRA-R spans from 65.0° to 196.9° E, -65.0° to 19.4° N (Figure 11~~Figure 1~~), with constant latitude and longitude increments of 0.11° × 0.11° ~~(approximately 12 km)~~ and 1200 × 768 grid points in the horizontal. The model was run to produce 12-hour (12h) forecasts in each 6-hourly cycle (see Section 2.2) to give extra data for ~~the~~ driving ~~aforementioned~~ dynamical downscaling within the domain.

The model parametrizations ~~of sub-grid scale processes (in convection, surface, boundary layer and mixed-phase clouds)~~ in BARRA-R are inherited from the UKMO Global Atmosphere (GA) 6.0 configurations described in Walters et al. (2017a). The GA6 configurations are also suited for limited-area models with resolutions > 10 km, but with some modifications~~. Several modifications have been implemented~~:~~,~~

i. A variable Charnock coefficient is used in surface heat exchange over the sea to improve the tropical Pacific air-sea exchange (Ma et al., 2015).

ii. The heat capacity of "inland water canopy" is set to 2.11×10^{7} J K^{-1}m^{-2} for modelling lakes. This ~~, which~~ improves the diurnal cycle over ~~the~~ inland waters. By contrast, grid cells containing salt lakes in Australia are modelled as bare soil surface (for Lake Eyre and Lake Frome) and vegetated surface (e.g., Lake Lefroy, Lake Ballard).

iii. For its deep convective mass flux scheme, a grid-box dependent convective available potential energy (CAPE) closure scheme is chosen to limit the role of parameterized convection. When vertical velocity exceeds the given threshold of 1 m/s, the vertical velocity dependent CAPE closure is chosen to release the convective instability efficiently (Zhu and Dietachmayer, 2015). These changes aim to improve the model stability.

iv. The river routing scheme has been turned off because it is not designed for a limited-area model. Therefore, there is no routing of runoff from inland grid points out to sea and inland water bodies, and soil moisture is not affected by this hydrological process.

The characteristics of the lower boundary, climatological fields and natural and anthropogenic emissions are specified using static ancillary fields. These are created as per Walters et al. (2017a, Table 1), with the exceptions of the land-sea mask and canopy tree heights. The land-sea mask is created from the 1 km resolution International Geosphere–Biosphere Programme (IGBP) land cover data (Loveland et al., 2000), and the canopy tree heights are derived from satellite light detection and ranging (LiDAR, Simard et al., 2011; Dharssi et al., 2015). Climatological aerosol fields (ammonium sulphate, mineral dust, sea salt, biomass burning, fossil-fuel black carbon, fossil-fuel organic carbon, and secondary organic (biogenic) aerosols) are used to derive the cloud droplet number concentration. Absorption and scattering by the aerosols are included in both the shortwave and longwave.

2.1.1 Land surface

The UM uses a community land surface model, the ~~The~~ Joint UK Land Environment Simulator (JULES, Best et al., 2011) ~~is the physically-based land surface component of the UM~~. It models partitioning of rainfall into canopy interception, surface runoff and infiltration, and uses the Richards' equation and Darcy's law to model soil hydrology. Sub-grid scale heterogeneity of soil moisture is represented by the Probability Distributed Moisture (PDM) model (Moore, 2007). A nine-tile approach is used to represent sub-grid scale heterogeneity in land cover, with the surface of each land point subdivided into five vegetation types (broadleaf tree, needle-leaved trees, temperate C3 grass, tropical C4 grass and shrubs) and four non-vegetated surface types (urban, inland water, bare soil and land ice). It describes a 3 m soil column with a 4-layer soil scheme with soil thicknesses of 0.1, 0.25, 0.65 and 2.0 m, and models vertical heat and water transfer within the column with van Genuchten hydraulic parameters. The JULES urban parameters are optimised for Australia as described by Dharssi et al. (2015).

2.1.2 Soil moisture

For the 1990-~~ to ~~2014 period, soil moisture fields in BARRA-R are initialised daily at every 06 UTC using soil moisture analyses from an offline simulation of JULES, at 60 km resolution, driven by bias corrected ERA-Interim atmosphere forcing data, using methods described in Dharssi and Vinodkumar (2017) and Zhao et al. (2017). The simulation used a 10-year long spin-up period and then was run continuously for the 1990 to 2014 period. The near-surface soil moisture analyses are found to have good skill for the Australian region when validated against ground-based soil moisture observations (Dharssi and Vinodkumar, 2017). As the offline runs were terminated at the end of December 2014, the daily initialization scheme is continued ~~For 2015 and onward, soil moisture fields in BARRA are initialised daily at every 06 UTC using~~with ~~40 km resolution~~ soil moisture analyses from the Bureau's global NWP system – ACCESS-G (Bureau of Meteorology, 2016). These external soil moisture analyses are downscaled to the BARRA-R grid using a simple method that takes into account differences in soil texture. ~~The daily initialisation was conducted with the purpose of avoiding spurious drift in the BARRA moisture fields.~~ As well, in each 6-hourly cycle, a land surface analysis is conducted within BARRA (see Section 2.2). The daily initialisation was conducted with the purpose of avoiding spurious drift in the BARRA moisture fields and reducing the time needed to spin up from ERA-Interim initial conditions. However, as multiple parallel production streams are needed to produce the reanalysis (see Section 2.2), a ~~a~~discontinuity in soil moisture in the bottom two layers exists between successive production streams, although soil moisture in the top two layers become stable after one-month of runs. A discontinuity occurring~~ring~~ at the 2014-2015 changeover has recently been reported by BARRA data users. These impacts, particularly on forested regions where trees extract water from the deep soil layers, are under investigation.

2.1.3 Boundary conditions

The BARRA-R sequential data assimilation process is initialized using ERA-Interim analysis fields (see Section~~.~~ 2.2), after which the only relationship with ERA-Interim is solely through the lateral boundary conditions. Hourly lateral boundary conditions for BARRA-R are interpolated from ERA-Interim's 6-hourly analysis fields at 0.75° × 0.75° resolution. The rim width of the boundary frame is 0.88°.

The land boundary is provided by a land surface analysis (Section~~.~~ 2.2). Daily sea-surface temperature (SST) and sea ice (SIC) analysis at 0.05° × 0.05° resolution from reprocessed (1985-2007, Roberts-Jones et al., 2012) and near real-time (NRT) Operational Sea Surface Temperature and Ice Analysis (OSTIA, Donlon et al., 2012) are used as lower boundaries over water after being interpolated to the UM grid. The NRT data is used from January 2007. OSTIA is widely used by NWP centres and operational ocean forecasting systems, owing to their short real-time latency. Even though the re-processed and NRT data do not constitute a homogeneous timeseries, OSTIA is favoured over other SST reanalyses owing to its higher spatial resolution. Masunaga et al. (2015, 2018) have shown steep SST gradients, unresolved by coarse SST reanalyses, can influence the organization of long-lived rain bands and enhancement or reduction of surface convergence, and this is particularly problematic for atmosphere-only reanalyses as thermal structure and motions in the marine atmospheric boundary lay~~t~~er are not well constrained by data assimilation.

2.2 Data assimilation system

The BARRA-R analysis scheme is based on fixed deterministic atmospheric and land surface assimilation systems used by the UKMO ~~for its UERRA~~in UERRA ~~reanalysis~~ (Jermey and Renshaw, 2016) and IMDAA ~~in the Indian Monsoon Data Assimilation and Analysis (IMDAA) reanalysis~~ (Mahmood et al., 2018). BARRA-R uses a sequential data assimilation scheme, advancing forward in time using 6-hourly analysis cycles centred at synoptic hours t_0 = 0, 6, 12 and 18 UTC, and 12h forecast cycles from t_0-3h (Figure 22~~Figure 2~~). ~~As noted before, longer-range forecasts are needed for driving the downscaling models.~~

In each analysis cycle, available observations, distributed across a 6h analysis window $t_0\text{-3h} \leq t < t_0\text{+3h}$, are combined with the prior information of the model forecast from the previous cycle (~~known as~~ the background state), to provide a more accurate estimate of the atmosphere over this window. This first involves a 4-dimensional variational (4DVar) analysis of the basic upper-air atmospheric fields (wind, temperature, specific humidity, pressure) with conventional and satellite observations (see below). 4DVar is favoured over 3DVar as it takes account of time tendency information in the observations and this has ~~significant~~ a positive impact on the resulting forecasts (Rawlins et al., 2007). The UKMO's VAR assimilation system (version 2016.03.0) is used. The 4DVar uses a linear perturbation forecast (PF) model (Lorenc 2003; Rawlins et al., 2007, Lorenc and Payne, 2007), which uses a simpler model state linearised about~~about~~ a 'guess' trajectory (i.e., tangent linear model) with a lower resolution (0.33° cf. 0.11°) than the full forecast model. The lower resolution is chosen to limit computational costs. The PF model uses a simplified set of physical parameterizations including a simple boundary layer, cloud latent heat release, large-scale precipitation and convection. In other words, it is assumed that the lower-resolution corrections to the background state (i.e. increments), interpolated to a higher resolution, are suitable corrections for the full model. The analysis increments from 4DVar valid at t_0-3h are added to the background state at t_0-3h to produce an improved initial condition for the forecast model to perform the next 12h forecast from t_0-3h to t_0+9h. A constraint of zero analysis increments is specified at the model boundary such that BARRA-R relies on the driving model ERA-Interim to define large-scale flow and other atmospheric conditions (Section 2.1.3).

The variational method ~~of assimilation~~ minimises a cost function whose two principal terms penalise distance to the background state and distance to the observations. The two terms are squared differences weighted by the inverse of their corresponding error covariances. In BARRA-R, the background error covariance has been estimated by a smooth parameterised approximation to climatology tuned by forecast differences (Ingleby, 2001). Accordingly, the estimated background error covariance is invariant between successive analysis windows, but is time varying within the analysis window. The cost function also includes a pressure-based energy norm that serves as a weak constraint digital filter to suppress spurious fast oscillations associated with gravity-inertia waves produced in model forecasts when analysis increments are added to the background state (Gauthier and Thépaut, 2001).

The initial land surface state can have a significant impact on short-term forecasts of screen-level temperature and humidity, and ~~the~~ its quality ~~of the initial state~~ can also be improved through data assimilation. An Extended Kalman Filter (EKF) using observations of 2 m temperature and humidity is used to analyse the BARRA land state at every 6 hour cycle and provide analyses of soil moisture, soil temperature and skin temperature as described by Dharssi et al. (2012). The assimilation of satellite~~- microwave~~ retrieved soil moisture is not attempted here as it has not been ~~implemented~~ realised in ACCESS. The UKMO's SURF analysis system (version 2016.07.0) is used to perform EKF. The Jacobian, which relates observed variables to model variables, for the Kalman gain matrix is estimated using finite difference by perturbing each model variable to be analysed in 40 perturbations and performing short 3-hour forecasts. Here JULES (version 3.0) is run in the standalone mode, decoupled from the UM. The BARRA-R land state is reconfigured with EKF-derived surface analyses at every t_0.

Notice that the last 6h forecast of this model run represents the prior state estimates needed for the next analysis cycle. The forecast fields valid at t_0-3h, t_0-2h and t_0-1h are discarded, as these fields may still be influenced by transient artefacts due to the slight imbalance introduced by the addition of the analysis increments. It is already noted that this effect is also mitigated with the energy norm in the 4DVar's cost function that penalises the unbalanced structure in the increments.

The reanalysis is produced with multiple parallel production streams to speed up production. Each stream has a month of spin-up time from the ERA-Interim initial conditions before production data is archived, with most streams producing~~ed~~ one year of reanalyses. ~~.~~Trials ~~undertaken at the Met Office~~ have shown that a one-month period is sufficient for spin-up the atmosphere (Renshaw et al., 2013) and top levels of soil moisture, but ~~. Most streams are set up to produce one year of reanalyses, excluding the first month of spin-up.~~insufficient for soil moisture in the deeper layers.

2.3 Observations

Conventional observations from ~~(namely,~~ land surface stations, ships, drifting buoys, aircrafts, radiosondes, wind profilers,~~)~~ and satellite observations, namely ~~(~~retrieved wind, radiances and bending angle~~) observations,~~ are assimilated in BARRA-R. The various observational types are chosen as they have been assimilated in the Bureau's operational NWP systems; other observational types, such as clear-sky radiances, have not been assimilated due to ~~time~~ resource constraints~~ to set them up~~. Rain observations from radar and gauges are also not assimilated as their assimilation schemes are still being tested for operational NWP. As listed in Table 1~~Table 1~~, the data sets are pragmatically taken from multiple sources, as they are being prepared during the production runs. Most of the observations prior to ~~2003~~ 2009 are supplied by ECMWF, and the satellite radiance data from~~those between 2003 to 2009 and conventional observation data from~~ 2017 and onwards~~03~~ are extracted from the UKMO operational ~~operational~~ archive~~s~~.

Formatted: Font: Bold

The Bureau's archived observational data is also used to support this work, especially for the cycles from 2010~~ and~~ onwards.~~.~~ ~~We~~ BARRA-R also assimilates additional high frequency (10 min) land surface observations from automatic weather stations in Australia, and locally derived satellite atmospheric motion vectors (AMV). ~~All the satellite data from 2010 onwards is taken from the Bureau's operational archives.~~ Ground positioning system (GPS) radio occultation bending angle data up to 2009 is provided by the Radio Occultation Meteorology Satellite Application Facility (ROM SAF)~~ and is extracted from the Bureau's archives for the time period since 2010~~. Additional land surface observations over New Zealand are extracted from their

National Climate Database (CliFlo, 2017). The 4DVar assimilation of local AMV (Le Marshall et al., 2013) and GPSRO (Le Marshall et al., 2010) has been shown to improve operational forecasts.

Before being assimilated, observations are screened to select the best quality observations, remove duplicates and reduce data redundancy via thinning, using the UKMO's Observing Processing System (OPS~~ system~~) (based on version 2016.03.0) (Rawlins et al., 2007). There are per-cycle quality controls performed based on the method of Lorenc and Hammon (1988). Observations significantly different from the model background are rejected when exceeding a threshold calculated by a Bayesian scheme, unless they are consistent with other observations nearby. The observational error variances and thinning distances are established at the UKMO and the Bureau for their NWP systems. For the surface, sonde and aircraft observations, an observation automatic monitoring system performs monthly blacklisting of sites that show consistently large differences with BARRA-R's forecast over a one-month period. The system also calculates bias corrections for surface pressure and for aircraft and sonde temperature.

For the satellite data, instruments and their individual channels are rejected when they become unreliable. The blacklisting is informed by the work of ECMWF and MERRA-2 reanalysis teams~~ for their reanalyses~~. Further, airmass-dependent variational bias correction is applied to satellite radiances as part of the assimilation process, allowing the time-varying corrections to fit drifts in instrumental bias (Harris and Kelly, 2001; Dee and Uppala, 2008). The bias corrections were calculated monthly, with the satellite radiances during the first month of each production stream not assimilated. There are abrupt changes to the amount of satellite data assimilated at the start and end of satellite missions and the various observational data archives.~~;~~ I~~i~~n some cases, ~~abrupt~~ changes occur when corrections were made to the observation screening and thinning rules mid-production of the 2010-2015 reanalyses. The impacts of such changes, known to cause artificial shifts and spurious trends in a reanalysis (e.g., Thorne and Vose, 2010; Dee et al., 2011)~~these~~ are still to be investigated for BARRA-R.~~.~~

3 Preliminary evaluation ~~of ten-year regional reanalysis~~

Our evaluation focuses on three areas:~~,~~ surface variables, pressure-level temperature and wind, and precipitation. For the surface variables, we compare BARRA-R against point-scale observations and gridded analyses of observations for 2 m temperature. For the pressure levels, we evaluate BARRA-R against point-scale observations of temperature and wind, and examine the timeseries of the bias between BARRA-R and the global reanalyses. Finally, as rain observations are not assimilated in BARRA-R, gridded analyses of rain observations from gauges and satellites are used to provide the best independent reference in this study.

Formatted: Normal, Space Before: 0 pt, After: 0 pt, Line spacing: single

~~**3.1 Analysis departure statistics**~~

~~The observation departure statistics of the analysis can be compared against those of the model background state (Sec. 2.2) to indicate how closely the reanalysis fits the observational data before and after an analysis cycle. Root-mean-squared difference (RMSD) and additive bias (bias, for brevity) are used to measure the departures for a wide range of observed fields, where bias is calculated as~~ $E(d_m) - E(d_o)$, ~~where~~ $E(*)$ ~~yields the expectation in time,~~ d_m ~~refers to the timeseries of model values and~~ d_o ~~are the observed values. Table 2 reports the ten-year mean values of the RMSD and bias for surface, sonde, aircraft-based and satellite wind fields. The assimilation process is behaving as desired by drawing the model towards the observations by reducing the RMSD and the magnitude of the bias for nearly all observational types. Monthly timeseries of the departure statistics, shown in the Supplementary Material, also suggests that this is achieved across the period.~~

3.1~~2~~ Surface

~~**The advantages of BARRA-R over global reanalyses are most likely to be found near the surface, as BARRA-R resolves near-surface features larger than**~~**down to** ~~**12 km in scale and assimilates more surface observations over Australia and New Zealand. This section first presents a point-scale evaluation of BARRA-R against surface observations, followed by comparison with gridded climate data**~~**analyses from observations**~~.~~

Formatted: Heading 2, Line spacing: 1.5 lines

3.1~~2~~.1 Point-scale evaluation of 2 m temperature, 10 m wind speed and surface pressure

The t_0+6h model forecasts of ~~screen (~~2 m~~)~~ (screen) temperature, 10 m wind speed and surface pressure are evaluated against land observations. These observations have only an indirect relation to the forecasts as they ~~These forecasts have some independence from the observations as they~~ are not used in the analysis for~~of~~ the associated cycle t_0. Since errors tend to grow with the forecast range, the assessment ~~estimates~~ places an upper bound on the true errors of the analysis fields between time t_0 and t_0+3h. These fields are interpolated ~~between~~from the ~~model's~~ model levels using surface similarity theory (Walters et al., 2017a). T~~The~~ he ERA-Interim t_0+6h forecasts from 0 and 12 UTC ~~are also evaluated to serve as a benchmark, where its forecasts are performed twice daily from 0 and 12 UTC~~and ~~.~~ the MERRA-2 hourly time-averaged forecast fields (M2T1NXSLV) are also evaluated to serve as benchmarks. It is not ideal to directly compare ~~two~~ reanalyses with different resolutions, and interpolating them onto common (observed) locations ~~before evaluation~~ diminishes some of the improvement achieved by BARRA-R relative to ~~ERA-Interim~~coarser reanalyses. Nonetheless, we undertake the latter to assess whether the models contain ~~information at the higher~~finer~~-~~scale information captured by point measurements; it therefore does not provide an assessment of the true quality of the ~~models~~ reanalyses at their native resolutions.

To correct representativity errors in both reanalyses, their model ~~fields~~ values at (modelled) land ~~points~~ grid cells are interpolated to the observation times and the station locations via bilinear interpolation in time and in the horizontal direction.

Height corrections are applied to the interpolated fields to match the station heights: the corrections to the screen temperature is based on dry adiabatic lapse rate (Sheridan et al., 2010), 10 m wind speed is based on Howard and Clark (2007), and the correction to surface pressure is based on the hydrostatic equation under a constant lapse rate. As the observations are irregularly distributed in time, we consider all observations within a t_0+5h to t_0+7h time window, with t_0 being 0 and 12 UTC, and the model grids are linearly interpolated to the observation times. Root-mean-squared difference (RMSD), Pearson's linear correlation, additive bias and variance bias are calculated at each station, with ~~the~~ $bias = mean(d_m) - mean(d_o)$, the variance bias ~~being calculated~~ as $Mbias = var(d_m)/var(d_o) - 1$ to capture differences in the dispersion, where $var(*)$ computes~~s~~ the variance in time. ~~The correlation assesses the temporal mismatch between the model and observations.~~

Boxplots in Figure 3 show~~s~~ the distribution of scores across 900-1500 stations in the BARRA-R domain~~ in boxplots~~. BARRA-R shows better agreement with the point observations than ~~ERA-Interim~~ the global reanalyses for ~~most~~ all three surface variables ~~and~~ by most of the measures. This result~~It~~ is expected since~~from the fact that~~ BARRA-R resolves near-surface features below 50 km horizontal scale, and assimilates more surface observations over Australia and New Zealand. ~~BARRA-R's screen temperature shows higher correlation and lower biases.~~ In particular, BARRA-R shows lower RMSD ~~than ERA-Interim~~ at ~~over~~ about 80% of the stations for screen temperature and 10 m wind speed, and at 70% of stations for ~~10 m wind speed and~~ surface pressure (see the Supplementary Material). At closer inspection in Figure 4(a), a percentile comparison plot of screen temperature deviation from monthly mean~~, shown in Figure 4(a),~~ indicates that the frequency distribution of BARRA-R temperature is closer to that of the observations than ERA-Interim, particularly in regimes below 25% percentiles and above 90~~5~~% percentiles.

For 10 m wind speed, negative biases for variance exist in ~~both~~ all the reanalyses~~, but less so for BARRA-R~~. Figure 4(b) shows that 10 m wind speeds~~they~~ are positively biased during light~~ow~~ wind conditions and vice versa during strong wind speeds. There are many possible reasons for under-estimating strong winds: the inaccurate descriptions of boundary layer mixing and form drag for sub-grid orography, and of surface properties such as land cover and vegetation types. Changing the fractional area of the vegetation canopy modifies scalar roughness of the vegetated tiles, affecting the wind speed. The seemingly linear variation in wind speed is known in the global reanalyses (e.g., Carvalho et al., 2014), and Rose and Apt (2016) attributed the problem of wind underestimation to inaccuracy in modelling wind speeds in unstable atmospheric conditions.

Pressure is a large-scale variable which is likely to be better represented by a global model than a limited-area model. However, ~~, although~~ the BARRA-R estimates of point-scale surface pressure are more accurate in topographically complex regions and coast~~-~~lines (see the Supplementary Material), where ~~ERA-Interim~~the estimates from the coarser reanalyses are ~~poor~~less representative~~, so that the inter-quartile range of the RMSD scores for BARRA-R is significantly narrower than for ERA-Interim~~.

3.1~~2~~.2 Comparison~~s~~ with gridded analysis of observed 2 m temperature

The reanalyses are compared against a gridded daily 0.05° × 0.05° analysis of station maximum and minimum 2 m temperature data from the Australian Water Availability Project (AWAP, Jones et al., 2007). The AWAP grids are generated using an optimised Barnes successive-correction method that applies weighted averaging of the station data. Topographical information is included by using anomalies from long-term (monthly) averages in the analysis process. The analysis errors for maximum temperature are larger near the coast around northwest Australia and around the Nullarbor Plain, due to strong temperature gradients between the coast and inland deserts and a relatively sparse network (Jones et al., 2007). The coast of Western Australia and parts of Northern Territory are likely to share this similar analysis issue. The analysis errors are greater for minimum temperature, especially over Western Australia and the Nullarbor Plain.

Figure 5 shows the differences for~~in~~ 2007-2016 ~~ten-year mean~~averages in daily maximum and minimum temperature from AWAP, ERA-Interim, MERRA-2 and BARRA-R. The daily statistics are derived from 3-hourly forecast fields of ERA-Interim and hourly fields of MERRA-2 and BARRA-R. While inherent biases due to sampling are expected, this comparison also ~~distinguishes~~ highlights the advantage of higher frequency data ~~generally found in a regional reanalysis~~ when examining lower and upper tail statistics. ~~The spatial variation in BARRA-R is very similar to AWAP, especially across the eastern seaboard of Australia where Eastern Highlands are the major driver for temperature variability. The insets show the contrasts from AWAP when the reanalyses are downscaled to the AWAP grid.~~ BARRA-R shows cold and warm biases (relative to AWAP) of around 1 K in daily maximum and minimum temperature respectively, particularly over the eastern region. MERRA-2 also shows similar levels of biases but with different signs and variability. ~~Despite this,~~ BARRA-R and MERRA-2 ~~shows better agreement~~agree better with AWAP than ERA-Interim, which reports differences (in mean) up to 5 K in magnitude. The reduced amplitude of~~in screen~~ the diurnal cycle of temperature is a long-standing problem in the UM; experiments ~~undertaken by UM development partners~~ have shown that changes to the representation of the land surface (e.g., reductions in the amount of bare soil and changes to scalar roughness and albedo of vegetated tiles) reduce clear-sky biases (Bush et al., 2019~~8~~).

Figure 6 shows the monthly means of the differences in daily maximum and minimum temperature between the reanalyses and AWAP averaged across Australia. Here the OSTIA SST anomaly timeseries is also included, and it does not show a visible discontinuity at 2006/2007 (Section 2.1.3). The maximum temperature in BARRA-R appears cooler than AWAP after a strong La Nina event in 2010-2011, while the global reanalyses also show cooler trends in biases after 2010. BARRA-R and ERA-Interim show smaller levels of temporal variability than MERRA-2. The minimum temperature in BARRA-R does not show an obvious trend but is warmer during 2010-2011 when ERA-Interim and MERRA-2 are cooler. These changes do not coincide with our changes in soil moisture initialization in 2014-2015 (Section 2.1.2) or OSTIA SST.

3.2~~3~~ Pressure levels

To assess BARRA-R in the atmosphere, we compare the t_0+6h forecasts on pressure levels ~~from BARRA-R~~ with radiosonde and pilot wind observations at 0 and 12 UTC on standard pressure levels ranging from 1000 to 10 hPa, using the harmonized data set produced by Ramella Pralungo et al. (2014a; 2014b). The pressure-level fields of BARRA-R and ERA-Interim's analyses at time t_0 are also compared, even though they are not independent from the observations; such comparisons only provide baselines to interpret the relative quality of the BARRA-R forecasts. Similar comparisons with ~~the~~ ERA-Interim's twice-daily forecasts at these observation times are also not possible because they start from 0 and 12 UTC. The model data is interpolated horizontally to the sonde and pilot launch locations via bilinear interpolation, and ~~the~~ RMSD is calculated at each location and pressure level. T~~.~~

~~Evaluations are undertaken at pressure levels ranging from 1000 to 10 hPa, and t~~he resulting boxplots of RMSD are shown in Figure 76~~Figure 6~~. Depending on the pressure level and parameter evaluated, between 54 to 203 sites were available. There is a marked variability in RMSD with the pressure levels, particularly for wind speed, due to ~~a range of~~ reasons such as variations in the number of observing sites, increasing sonde drift error on ascent, and differences in dynamic range of the fields with height. A markedly higher RMSD for wind speed occurs at ~~height of~~ 200 hPa where the jet stream can occur.

It is difficult to discern the differences between the two analyses, suggesting that they perform similarly from assimilating the same observations. Assimilation at a coarser resolution of 0.33° (cf. 0.11° of the forecast model) in BARRA-R does not drastically improve 0.75° representations of temperature and wind at these pressure levels and at point scales. There are also small differences between the analyses and BARRA-R background, indicating that the 0.11° forecast model does not degrade from the lower-resolution analysis of BARRA-R but also does ~~also~~ not improve upon the ERA-Interim's 0.75° representation of these fields at the observation locations.~~.~~

Figure 8 compares BARRA-R's 0 UTC analysis of air temperature at 850, 700 and 500 hPa against the analyses from ERA-Interim and MERRA-2 (M2I3NPASM). BARRA-R is cooler at 500 hPa across the domain, and warmer at 850 hPa in the tropics than the global reanalyses, and the monthly differences in the zonal mean are of order 1 K. BARRA-R also shows a cooling shift at 700 and 500 hPa in the tropics, and a warming shift over south of 40°S after 2010. But when compared against MERRA-2, in the tropics, BARRA-R is warmer at 700 hPa, and the apparent shift in BARRA-R is also seen in~~inconclusive as~~ MERRA-2 ~~also shows similar shifts~~ (relative to ERA-Interim) at these levels.

3.3~~4~~ Precipitation

We consider three reference gridded data sets to compare with the reanalyses. First is the 0.05° × 0.05° rain gauge analysis of daily accumulation over Australia from AWAP, produced using the Barnes method where the ratio of observed rainfall to monthly average is used in the analysis process (Jones et al., 2009). There is a north-south gradient in the AWAP analysis errors with larger analysis errors in the northern tropical regions, where length scales of convective rainfall events are shorter and more variable (Jones et al., 2009). Second is the 1° × 1° (full data daily) rain gauge ~~(~~analysis over the domain from the Global Precipitation Climatology Centre (GPCC version 2018, Ziese et al., 2018), created using an empirical weighting-based interpolation method described in Becker et al. (2013). As with AWAP, GPCC is less accurate in regions where station scarcity and high precipitation variability coexist. For instance, different GPCC interpolation methods can yield~~s~~ very different analyses over the south Asia region (Becker et al., 2013). The third reference is the 0.25° × 0.25° satellite-based analysis of 3-hourly rain rates from the Tropical Rainfall Measuring Mission (TRMM) multi-satellite precipitation analysis (TMPA 3B42 version 7, Huffman et al., 2006). TMPA 3B42 combines precipitation estimates from various satellite systems and rain gauge monthly analysis. Satellite-derived estimates of convective precipitation are largely accurate in the low latitudes (Ebert et al., 2007, Chen et al., 2013), but the TMPA product is less accurate over the ocean due to the absence of local observations used for gauge adjustments (Sapiano and Arkin, 2009), and south of 40°S due to limited local cross-sensor calibration (Huffman et al., 2008). TRMM often underestimates precipitation in high-latitude regions with significant topography due to difficulties of satellite retrievals over snow covered surfaces and/or due to the high elevations (Barros et al. 2006; Matthews et al. 2013). TRMM is also known to underestimate~~miss amount of~~ light rainfall and drizzle over subtropical and high-latitude oceans (Berg et al., 2010). In addition to these considerations, there are inherent limitations in comparing the reanalyses with AWAP, GPCC and TMPA. Specifically, products with coarser grids tend to over-represent low-threshold events occurring at spatial scales smaller than their grid sizes and under-represent high-threshold events. Further evaluation of BARRA-R precipitation estimates against point gauge observations and AWAP are reported in Acharya et al. (2019).

~~Rain observations are not assimilated in either~~ Neither BARRA-R nor~~or~~ ERA-Interim assimilated rainfall observations. Precipitation estimation ~~within~~ from their forecast models is constrained by other observation types~~s~~. Following Section 2.1, in BARRA-R, the microphysics scheme based on Wilson and Ballard (1999) parameterises the atmospheric processes that transfer water between the four modelled states of water (vapour, liquid droplets, ice, and raindrops) to remove moisture resolved on the grid scale. As the 12 km model is not "storm resolving", BARRA-R uses the mass flux convective parameterization scheme of Gregory and Rowntree (1990) with the CAPE closure to model sub-grid scale precipitating and non-precipitating~~on~~ convection using an ensemble of cumulus clouds as a single entraining-detraining plume. Such a scheme prevents ~~. The UM uses the microphysics scheme based on Wilson and Ballard (1999) to form and evolve precipitation due to grid-scale processes (Walters et al., 2017a). For sub-grid scale processes, it uses a mass flux convective parameterization scheme with the CAPE closure (Gregory and Rowntree, 1990) to produce the convective-scale motion (< 10 km) and thus prevent~~ unstable growth of cloudy structures on the grid, which is otherwise required for explicit vertical circulations to develop (Clark et al., 2016). The modelled convection~~latter~~ also works independently at each grid point, and the model can only predict the area-average rainfall, instead of the spectrum of rainfall rates. ~~In other words~~Consequently, BARRA-R's precipitation estimates from sub-grid convection ~~processes~~ will be more erroneous than those for large-scale precipitation. In other words,

~~The~~ the accuracy of BARRA-R is expected to ~~poorer~~ worsen during the warm season and at low latitudes, ~~while~~ and to improve~~better~~ during cooler season and at high latitudes where non-convective precipitation is dominant. To allow the UM to spin-up from the ~~0.33°~~ analysis increments, we examine the quality of the precipitation accumulation between t_0+3h to t_0+9h, by comparing against gridded data sets. This also addresses the issue that the UM ~~has~~ yields ~~an~~ excess ~~of~~ precipitation at analysis time (t_0-3h) due to a temporary imbalance in the moisture fields, by allowing time for the model to adjust and~~to~~ remove the excess.

For ERA-Interim, we used its first 12h accumulation, which ~~because it~~ is considered the most accurate (Kallberg, 2011). ~~We examine BARRA-R and ERA-Interim with 0.05° × 0.05° raingauge analysis of daily accumulation from AWAP and 0.25° × 0.25° satellite-based analysis of 3-hourly rain rates from the Tropical Rainfall Measuring Mission (TRMM) multi-satellite precipitation analysis (TMPA 3B42 version 7, Huffman et al., 2006). The AWAP rain grids are also produced using the same Barnes method, where the ratio of observed rainfall to monthly average is used in the analysis process. Some areas in AWAP have been masked (shown in white) because there were insufficient observations to derive reliable estimates. There are limitations in comparing datasets with different grids. Specifically, products with coarser grids tend to over-represent low-threshold events occurring at spatial scales smaller than their native grid sizes and under-represent high-threshold events.~~

3.3.1. Mean annual precipitation and frequency of rain days

Figure 97,~~The first column in Figure 7~~ row (i) compares the ten-year (2007-2016) annual mean precipitation ~~amount~~ estimated from the five~~our~~ data sets. A close-up over Australia can be found in the Supplementary Material. BARRA-R provides a realistic depiction when compared with TMPA across the domain, ~~,~~ but show~~ings~~ higher precipitation over the tropics and over the Tasman Sea and Southern Ocean. ~~By contrast, ERA-Interim shows even higher precipitation over the tropics and insufficient rain over the Tasman Sea. TMPA is expected to be less accurate over the ocean due to the absence of local observations used for gauge adjustments (Sapiano and Arkin, 2009), and south of 40°S due to limited local cross-sensor calibration (Huffman et al., 2008).~~ BARRA-R ~~also~~ agrees very well with AWAP and GPCC over Australian land areas, reflecting the markedly higher precipitation in the northern tropics, and western Tasmania. It also agrees with GPCC over New Zealand. ~~Notice the discrepancy between AWAP and TMPA over Tasmania, suggesting possible negative biases in TMPA in high-latitude regions with significant topography due to difficulties of satellite retrievals over snow covered surfaces and/or due to the high elevations where TMPA often underestimates precipitation (Barros et al. 2006; Matthews et al. 2013).~~ BARRA-R also shows better agreement with AWAP, GPCC and TMPA in some of the dry areas such as western Australia.

The frequency of days with three intensity regimes is examined next in Figure 97. First in row (ii), we examine the frequency of light rain days with amounts between [1,10) mm.~~,~~ ~~with t~~The 1 mm threshold ~~being~~ is chosen~~. This~~ to account~~s~~ for the tendency of the model to create light "drizzle" events with very low rain rates. Even so, the two reanalyses show significantly more rain days in the tropics than TMPA and GPCC, and more rain days than TMPA over the Southern Ocean. ~~Comparing~~

Formatted: Heading 3, Space Before: 0 pt, After: 0 pt

~~with TMPA, the two reanalyses tend to show significantly more rain days in the tropics, western Tasmania, and the Southern Ocean.~~ TRMM is known to miss light rainfall events over subtropical and high-latitude oceans ~~miss amount of light rainfall and drizzle over subtropical and high-latitude oceans~~ (Berg et al., 2010), while simulated precipitation over the Southern Ocean over-estimates drizzle ~~(Franklin et al., 2013; Wang et al., 2015)~~ when compared with satellite observations (Franklin et al., 2013; Wang et al., 2015). Some of these differences from TMPA are not mirrored by AWAP over Australia, suggesting possible under-estimation of rain days in TMPA over land (e.g., eastern seaboard, southwest Australia) wher~~ee~~e the gauge network is relatively dense (see the Supplementary Material). Despite these considerations, BARRA-R over-estimates the frequency of light rain days when compared with AWAP, notably in the northern and central regions of Australia, and Tasmania. The UM's parameterized convection scheme assumes that there are many clouds per grid box – which is marginal at the BARRA-R's resolution, and thus produces a bias towards widespread precipitation and has little indication of the areas which could expect larger rain rates (Clark et al., 2016).

Formatted: Not Highlight

Formatted: Not Highlight

For heavy precipitation days, with amounts [10,50) mm, Figure 97(iii) shows ~~there are~~ greater similarities between BARRA-R ~~and~~, AWAP and GPCC, over land regions such as southeast coast of Australia and Tasmania, than for ERA-Interim. ~~However,~~ BARRA-R shows differences from AWAP and GPCC ~~underestimates the frequency~~ over Australia north of 30°S where the gauge analyses are poorer.~~.~~ Over the ocean, the two reanalyses show more heavy precipitation days than TMPA in the tropics~~, although BARRA-R is more similar to TMPA~~.

~~Finally~~Lastly~~,~~ for the very heavy precipitation days (≥ 50mm) in Figure 97(iv), it is obvious that ERA-Interim does not fully capture the ~~enough~~ frequency over land in northern Australia, and southeast Asia, whereas BARRA-R is more comparable with the three reference datasets~~AWAP and TMPA.~~. This agrees with the findings of Jermey and Renshaw (2016) that higher-resolution regional reanalyses show improvement in representing high-threshold events at these spatial scales. ~~Over the land in northern Australia, there are discernible differences in spatial variability between AWAP and BARRA-R.~~ Over the ocean, BARRA-R also shows greater rainfall intensity in the tropics than ERA-Interim, but both reanalyses show lower intensity compared to TMPA. ~~Since satellite-derived estimates of convective precipitation are largely accurate in the low latitudes (Ebert et al., 2007, Chen et al., 2013), t~~These reflect the deficiency of the parameterized convection scheme in BARRA-R for estimating convective precipitation amounts in this region.

Formatted: Highlight

3.3.2. Comparison of monthly totals

Formatted: Heading 3, Space Before: 0 pt, After: 0 pt

Figure 108 and Figure 11 ~~Figure 8~~ compare~~s~~ differences in domain-averaged monthly totals between the reanalyses (BARRA-R and ERA-Interim) and reference data (TMPA and GPCC) ~~of the reanalyses with TMPA, on the TMPA grid~~ over five separate sub-domains between 80 to 180° E. Precipitation over land and ocean are distinguished. Over the tropical ocean between ±10°N [Figure 108, row (i)], the two reanalyses show different shifts in overall differences from TMPA at around

2010, and these shifts are not apparent in the other sub-domains. Across the sub-domains, the variances of the differences are similar between the two reanalyses.

Over tropical land regions, BARRA-R shows much higher totals than others [Figure 11(i)], due to higher precipitation occurring ~~being~~at high or sharp topographical regions in Papua New Guinea (PNG), Indonesia and Sumatra, and relatively small Indonesian islands (see the Supplementary Material). Other reanalyses and other gridded precipitation products disagree greatly at these locations with few observations and mountainous terrains (e.g., over PNG in Smith et al., (2013)). BARRA-R (and GPCC) also shows markedly higher monthly totals below 39.2° S [Figure 11(v)], than TMPA and ERA-Interim. This is due to higher BARRA-R precipitation estimates on the west coast and Southern Alps of New Zealand (see the Supplementary Material), where precipitation is likely underestimated in TMPA.

The UM can produce grid localized high precipitation in BARRA-R, especially in unstable atmospheric conditions over steep orographic slopes. This issue is not unique to the UM but for instance ~~-~~also occurs in the Weather Research and Forecasting model (Gustafson et al., 2014). When the convective parameterization in non-convective resolving models does not stabilize the air column, meteorological events can develop at the smallest resolvable scales in the model, producing unrealistically strong vertical velocities and precipitation; this is known as "grid-point storms" (Scinocca and McFarlane, 2004; Williamson, 2013). Such storms occur more readily in models with higher horizontal resolutions (Williamson, 2013). As the resolution increases, resolved motions can produce moisture convergence and increase CAPE very rapidly, and the rate at which column instability is produced depends on the scale of moisture and heat convergence. This also tends to occur over tropical ~~-~~land areas, over steep topography, and during the warm seasons, when the atmosphere is unstable and there is sufficient warm moisture supply at the surface. These considerations do not lend themselves to explain the observed bias in BARRA-R.

By contrast, BARRA-R shows ~~good~~ better agreement with ~~ERA-Interim~~GPCC and TMPA in other sub-domains ~~for tropical, subtropical and temperate regions~~ between 39.2° to 10.0° S~~outh~~ [Figure 11(ii-iv)]. Over the land between 23 to 10°S, ~~.~~ ~~BARRA-R shows significantly higher totals between ±10° over land, owing to occurrences of "grid-point storms". These can occur over high or sharp topographical regions, such as in Papua New Guinea, and Indonesia, and Pacific islands resolved only as single or few 0.11° × 0.11° cells. Numerical noise during computations can accumulate to trigger a fictitious storm by the convective parameterization scheme. The condensation heat release at the saturated grid box leads to a strong uplift. The model then removes this excess moisture in the column by generating very large precipitation localised at that grid cell. This is more likely to occur over land in the tropics and sub-tropics and during the warm seasons, when the atmosphere is unstable and there is sufficient warm moisture supply at the surface.~~ BARRA-R simulates wetter summer events than observed in TMPA and GPCC from 2011, when Australia was recovering from drought conditions with the onset of La Nina. Between 39 to 23°S, BARRA-R also simulated wetter events over Mt Kosciuszko, Tasmania, and North Island of New Zealand than TMPA after 2014. This over-estimation is however less apparent when BARRA-R is compared with GPCC.

~~BARRA-R also shows higher monthly totals below 39.2° South latitude over Tasmania and New Zealand, than TMPA and ERA-Interim. The discrepancy is partly due to (aforementioned) negative bias in TMPA and ERA-Interim in Tasmania, and occurrences of grid-point storms in BARRA-R over its high topography in New Zealand.~~

4 ~~Summary~~ Discussion and outlook

The recent development of ~~the~~ global and regional reanalyses addresses the need for high-quality, increasingly higher resolution, and longer-term reanalyses, accompanied by estimates of uncertainty~~ies~~, within the research and broader user communities. BARRA is the first ~~represents one of the latest global efforts to develop~~ regional reanalysis~~es, and is the only one to date~~ that focuses on the Australasian section of the Southern Hemisphere. It is developed with significant co-investment from state-level emergency service agencies across Australia, due to the advantages of deeper understanding of past weather, including extreme events, and especially in areas that ~~are~~ have been ~~currently~~ poorly served by observation networks. The 2~~8~~9-year BARRA reanalysis, which is expected to be completed ~~fully~~ in 2019, ~~will ultimately represent a collection of high-resolution gridded meteorological data sets with 12 km and 1.5 km lateral spatial resolution and 10 minutes to hourly time resolution. BARRA~~ will ultimately represent a collection of high-resolution gridded meteorological data sets with 12 km and 1.5 km ~~lateral spatial~~horizontal resolution and 10 minutes to hourly time resolution. ~~The production is well underway and is expected to complete in 2019.~~

In this paper, we describe the BARRA 12 km regional reanalysis – BARRA-R, which is closely related to the Bureau's regional NWP system, although with an updated UM, 4DVar, ~~(with~~ variational bias correction~~)~~ and automated station blacklisting systems ~~are used~~. BARRA-R covers a significant region of the globe including parts of South East Asia and the eastern Indian Ocean, the southwest Pacific, Australia and New Zealand and assimilates a wide range of conventional and satellite observations that have proven to improve the skill of NWP.

BARRA-R produces a credible reproduction of the meteorology at and near the surface over land as diagnosed by the selected variables. BARRA-R improves upon its global driving model, ERA-Interim, showing better agreement with point-scale observations of 2 m temperature, 10 m wind speed and surface pressure. Results are similar when BARRA-R is compared with MERRA-2. Daily maximum and minimum statistics for 2 m temperature at 5 km resolution are captured in BARRA-R with smaller biases than ERA-Interim. There appear to be shifts in biases, relative to land observation analyses, over Australia amongst all the reanalyses, mirroring ~~with~~ changes in SST. This behaviour however does not coincide with known changes to the forcing data (soil moisture and SST) used in BARRA-R and~~but~~ requires further analysis to be better understood. BARRA-R's 10 m wind fields show lower biases than ERA-Interim and MERRA-2, but the negative bias during strong winds, which is common amongst other reanalyses, remains significant. Altogether, BARRA-R provides good representation of near-surface extremes, which has implications for its uses for energy management, fire risk and storm damages. The~~is~~ bias could be addressed via post-processing using methods such as those~~at~~ of Glahn and Lowry (1972), and Rose and Apt (2016).

~~Altogether, BARRA-R provides better representation of near-surface extremes, which has implications for its uses for energy management, fire risk and storm damages.~~ More generally, a variety of post-processing methods can further improve the accuracy of BARRA-R data (e.g., Berg et al., 2012; Frank et al., 2018). Our study did not discern clear merits in BARRA-R analysis and forecast, relative to ERA-Interim analysis, for the pressure-level temperature and wind. Further, there is no conclusive explanation for the shifts in 500, 700 and 850 hPa air temperature occurring at 2010, as comparisons with ERA-Interim and MERRA-2 yield mixed results. Other evaluations of the UM GA6 configuration~~s~~ including tropical cyclones, precipitation, clouds and large-scale flow, are reported in Walters et al. (2017a; 2017b), albeit in global models at coarser spatial resolutions.

Precipitation fields from BARRA-R show similarities with AWAP and GPCC ~~AWAP's gridded daily~~ rain gauge analyses~~is~~ over Australia, where it reflects more similar frequency statistics for heavy rain events and annual mean than ERA-Interim. While this is expected from comparing grids with different ~~measurement~~ resolutions~~support~~, BARRA-R ~~is expected to~~ contains more information pertaining to rain events at local scales. The frequency statistics (of both light and heavy rain days) of the two reanalyses are markedly different from TMPA over regions exterior to Australia~~, even though the variability of the monthly totals is very similar amongst the reanalyses and TMPA across the domain~~. BARRA-R is likely to be positively biased over land in the regions north of 10° S and New Zealand due to higher precipitation estimates concentrated in regions with high or steep~~sharp~~ topography~~ical areas~~. This is partly due to the presence of grid-point storms that commonly occur in non-convective resolving models. Alas, ~~due to grid-point storms, but~~ the likely ~~TMPA precipitation~~ underestimation~~s~~ in observations associated with the high elevations ~~make this~~poses difficulties to quantify ~~through direct comparison~~the wet bias. The ~~distinct~~ characteristics of grid-point storms in terms of superficial spatial localization, precipitation amount and vertical wind speed, could be detected and screened out via post-processing. The disagreement with TMPA is also apparent over the oceans, but consensus between satellite-based products generally degrades over higher latitudes, especially over the S~~s~~outhern O~~o~~cean~~s~~ (Behrangi et al., 2014). ~~The distinct characteristics of grid-point storms in terms of superficial spatial localization, precipitation amount and vertical wind speed, could be detected and screened out via post-processing.~~ ~~During~~Over the ~~the~~ 2003-2016 period, the variability of the monthly precipitation totals is similar amongst the reanalyses, TMPA and GPCC across the domain. Notable exceptions are a dry shift occurring in BARRA-R at 2010 over the tropical ocean, and wetter summer events over land in ~~the~~northern and southeast Australia, and the North Island of New Zealand after 2014. These coincident shifts in daily maximum 2 m temperature (over Australia), upper-air temperature (across the BARRA-R domain), and tropical precipitation in all the reanalyses suggest larger differences in large-scale synoptic patterns after 2010.

~~More in-depth evaluation of BARRA-R precipitation estimates against point gauge observations and AWAP are reported in Acharya et al. (2018).~~

Higher resolution models used to downscale BARRA-R ~~would also~~could alleviate the observed~~se~~ shortcomings by resolving sharp topographical features, resolving sub-grid processes (e.g., convection), and using science configurations more suited for a given climatic region. Assessment of the UM's first Regional Atmosphere (RA1) science configurations for convective-permitting models, recently concluded in December 2017, distinguishes two different science configurations for mid-latitude and tropical regions (RA1-M and RA1-T respectively). Developments in RA1 have produced ~~can lead to~~ improvements to 2 m temperature, 10 m wind speed and precipitation (Bush et al., 2019~~8~~). Further, it is known that BARRA-R's convection scheme, involving instantaneous adjustment of cloud fields to changes in forcing (e.g., solar heating, land/sea temperature differences), can lead to unrealistic behaviour at places such as coasts and in time (e.g., incorrect diurnal cycle) (Clark et al., 2016). A companion article will examine the ~~relative~~ merits from downscaling ~~between downscaled regional reanalyses and~~ BARRA-R with convective-scale models.~~.~~

~~The recent development of the global and regional reanalyses addresses the need for high-quality, increasingly higher resolution, and longer-term reanalyses, accompanied by uncertainties, within the research and broader user communities. BARRA therefore represents the recent effort in the development of regional reanalyses, and is the first to focus on the Australasian region. It is developed with significant co-investment from state-level emergency service agencies across Australia, due to the advantages of deeper understanding of past weather, including extreme events, and especially in areas that are currently poorly served by observation networks. The 28-year BARRA reanalysis, which is expected to be completed fully in 2019, will ultimately represent a collection of high-resolution gridded meteorological data sets with 12 km and 1.5 km lateral spatial resolution and 10 minutes to hourly time resolution.~~

Finally, BARRA ~~also~~ represents an important step in supporting the Bureau's ability to prepare for future reanalysis-related activities such as data rescue and reprocessing of observational data. Future reanalyses could use higher resolution models and ensemble-based forecast and assimilation systems to quantify uncertainties. They will also benefit from international efforts in reprocessing historical conventional and satellite observations with enhanced quality and/or more accurate uncertainty estimates.

Code availability. All code, including the UM (version 10.2), VAR (version 2016.03.0), JULES (version 3.0), OPS (version 2016.03.0), SURF (version 2016.07.0) systems, used to produce BARRA is version-controlled under Met Office Science Repository Service. Readers are referred to https://code.metoffice.gov.uk/trac/home for access information.

Data availability. The first releases of the BARRA-R data set for period 2003~~10~~-2016~~5~~ are~~is~~ available for academic use, with subsequent releases planned for ~~late 2018 and~~ ~~early~~ mid-2019. Readers are referred to http://www.bom.gov.au/research/projects/reanalysis for information on available parameters and access.

Competing interests. The authors declare that they have no conflict of interest.

Author contribution. PS, DJ, PFH and CJW conceived and/or designed BARRA. CHS, NE and PS developed the BARRA system with inputs from SR, CF, ID and HZ. CHS and NE performed the production and evaluation. CHS prepared the manuscript with contributions from all co-authors.

Acknowledgements

Funding for this work was provided by emergency service agencies (New South Wales Rural Fire Service, Western Australia Department of Fire and Emergency Services, South Australia Country Fire Service, South Australia Department of Environment, Water and National Resources) and research institutions (Antarctic Climate and Ecosystems Cooperative Research Centre (ACE CRC) and University of Tasmania). Funding from Tasmania is supported by the Tasmanian Government and Australian Government, provided under the Tasmanian Bushfire Mitigation Grants Program.

BARRA-R is set up with assistance from the UKMO~~'s UERRA~~ reanalysis team (R. Renshaw, P. Jermey, J. Davis) and colleagues (A. Maycock, D. Walters, I. Boutle), and many colleagues at the Bureau of Meteorology (T. Le, I. Bermous, L. Rikus, C. Sanders, J. Lee, G. Dietachmayer, J. Le Marshall, X. Sun, G. Kociuba, C. Tingwell, H. Zhang), the Commonwealth Scientific and Industrial Research Organisation (CSIRO, M. Dix), National Computational Infrastructure (NCI, D. Roberts). We thank R. Renshaw for providing the observational data from the UKMO and ECMWF archives; S. Moore and T. Carey-Smith at National Institute of Water and Atmospheric Research (NIWA) for providing additional local observations over New Zealand; R. Smalley and D. Jones for~~on~~ their~~his~~ advice on AWAP; P. May, E. Ebert, ~~and~~ A. Dowdy and T. Hirst for their feedback on early drafts of manuscript. BARRA-R uses the ERA-Interim data, provided through ARC Centre of Excellence for Climate System Science (P. Petrelli) at NCI. Many of the observational data sets were provided by ECMWF, UKMO and NIWA. The radio occultation data were provided by the Radio Occultation Meteorology Satellite Application Facility (ROM SAF, through K. B. Lauritsen) which is a decentralized operational RO processing center under EUMETSAT. RO data are available at http://www.romsaf.org. This project was undertaken with the assistance of resources and services from NCI, which is supported by the Australian Government.

ERA-Interim can be retrieved from ECMWF, https://www.ecmwf.int/en/forecasts/datasets/archive-datasets/reanalysis-datasets/era-interim. AWAP data can be requested from, http://www.bom.gov.au/climate, ~~and~~ TMPA v7 data is retrieved via NASA Goddard Earth Sciences (GES) Data and Information Services Center (DISC), https://disc.gsfc.nasa.gov/datasets/TRMM_3B42_V7/summary, and GPCC v2018 data is~~.~~ retrieved from Deutscher Wetterdienst.

References

Acharya, S. C., Nathan, R., Wang, Q. J., Su, C.-H., and Eizenberg, N.: An evaluation of daily precipitation from atmospheric reanalysis products over Australia, Hydrol. Earth Syst. Sci. Discuss., https://doi.org/10.5194/hess-2018-607, in review, 2019. ~~in preparation.~~

Arakawa, A., and Lamb, V. R.: Computational design of the basic dynamical processes of the UCLA general circulation model. Methods of Comp. Phys.: Adv. Res. Appl., 17, 173–265, doi: 10.1016/B978-0-12-460817-7.50009-4, 1977.

Barros, A. P., Chiao, S., Lang, T. J., Burbank, D., and Putkonen, J.: From weather to climate—Seasonal and interannual variability of storms and implications for erosion process in the Himalaya. Geological Society of America Spatial Paper 398, Penrose Conference Series, 17–38, 2006.

Becker, A., Finger, P., Meyer-Christoffer, A., Rudolf, B., Schamm, K., Schneider, U., and Ziese, M.: A description of the global land-surface precipitation data products of the Global Precipitation Climatology Centre with sample applications including centennial (trend) analysis from 1901–present, Earth Syst. Sci. Data, 5, 71-99, https://doi.org/10.5194/essd-5-71-2013, 2013.

Behrangi, A., G. Stephens, R.F. Adler, G.J. Huffman, B. Lambrigtsen, and M. Lebsock: An update on the oceanic precipitation rate and its zonal distribution in light of advanced observations from space. J. Climate, 27, 3957–3965, doi: 10.1175/JCLI-D-13-00679.1, 2014.

Berg, W., T. L'Ecuyer, and J.M. Haynes: The distribution of rainfall over oceans from spaceborne radars. J. Appl. Meteor. Climatol., 49, 535–543, doi: 10.1175/2009JAMC2330.1, 2010.

Berg, P., Feldmann, H., and Panitz, H.-J.: Bias correction of high resolution regional climate model data. J. Hydrol., 448-449, 80-92, doi: 10.1016/j.jhydrol.2012.04.026, 2012.

Best, M.J., Pryor, M., Clark, D.B., Rooney, G.G., Essery, R.L.H., M´enard, C.B., Edwards, J.M., Hendry, M.A., Porson, A., Gedney, N., Mercado, L.M., Sitch, S., Blyth, E., Boucher, O., Cox, P.M., Grimmond, C.S.B. and Harding, R.J.: The Joint UK Land Environment Simulator (JULES), model description - Part 1: Energy and water fluxes. Geosci. Model Dev., 4(3) 677–699. doi:10.5194/gmd-4-677-2011, 2011.

Bollmeyer, C. , Keller, J. D., Ohlwein, C. , Wahl, S. , Crewell, S. , Friederichs, P. , Hense, A. , Keune, J. , Kneifel, S. , Pscheidt, I. , Redl, S. and Steinke, S.: Towards a high‐resolution regional reanalysis for the European CORDEX domain. Q. J. R. Meteorol. Soc., 141: 1-15. doi:10.1002/qj.2486, 2015.

Borsche, M., Kaiser-Weiss, A. K., Unden, P., and Kaspar, F.: Methodologies to characterize uncertainties in regional reanalyses. Adv. Sci. Res., 12, 207-218, doi: 10.5194/asr-12-207-201, 2015.

Borsche, M., Kaiser-Weiss, A.K., and Kaspar, F.: Wind speed variability between 10 and 116 m height from the regional reanalysis COSMO-REA6 compared to wind mast measurements over Northern Germany and the Netherlands. Adv. Sci. Res., 13, 151–161, doi: 10.5194/asr-13-151-2016, 2016.

Bromwich, D., A. Wilson, L. Bai, Z. Liu, M. Barlage, C. Shih, S. Maldonado, K. Hines, S.-H. Wang, J. Woollen, B. Kuo, H. Lin, T. Wee, M. Serreze, and J. Walsh: The Arctic System Reanalysis Version 2. Bull. Amer. Meteor. Soc., 99, 805-828, doi: 10.1175/BAMS-D-16-0215.1, 2018.

Brown, A., S. Milton, M. Cullen, B. Golding, J. Mitchell, and A. Shelly: Unified modeling and prediction of weather and climate: A 25-Year journey. Bull. Amer. Meteor. Soc., 93, 1865–1877, doi: 10.1175/BAMS-D-12-00018.1, 2012.

Bureau of Meteorology: Operational implementation of the ACCESS numerical weather prediction systems, NMOC Op. Bull. No. 83, accessed online, http://www.bom.gov.au/australia/charts/bulletins/apob83.pdf, 2010.

Bureau of Meteorology: APS1 upgrade of the ACCESS-R numerical weather prediction system, NMOC Op. Bull. No. 98, accessed online, http://www.bom.gov.au/australia/charts/bulletins/apob98.pdf, 2013.

Bureau of Meteorology: APS2 upgrade to the ACCESS-G numerical weather prediction system, BNOC Op. Bull. No. 105, accessed online, http://www.bom.gov.au/australia/charts/bulletins/APOB105.pdf, 2016.

Bush, M., et al.: The Met Office Unified Model Regional Atmosphere 1 and JULES Regional Land 1 configurations, in prep., 2018.

Carvalho, D., Rocha, A., Gomez-Gesteira, M., and Santos, C. S.: WRF wind simulation and wind energy production estimates forced by different reanalyses: comparison with observed data for Portugal, Appl. Energy, 117, 116-126, doi: 10.1016/j.apenergy.2013.12.001, 2014.

Charney, J. G, and Phillips, N. A.: Numerical integration of the quasi-geostrophic equations for barotropic and simple baroclinic flows. J. Meteorol. 10: 71–99, doi: 10.1175/1520-0469(1953)010<0071:NIOTQG>2.0.CO;2, 1953.

Chen, Y., E. E. Ebert, K. J. E. Walsh, and N. E. Davidson: Evaluation of TRMM 3B42 precipitation estimates of tropical cyclone rainfall using PACRAIN data, J. Geophys. Res. Atmos., 118, 2184-2196, doi: 10.1002/jgrd.50250, 2013.

Clark, P., Roberts, N., Lean, H., Ballard, S. P., and Charlton-Perez, C.: Review: Convection-permitting models: a step-change in rainfall forecasting, Meteor. App., 23, 165–181, doi: 10.1002/met.1538, 2016.

CliFlo: NIWA's National Climate Database on the Web, http://cliflo.niwa.co.nz, Data Retrieved: 17 February 2017.

Davies, T., Cullen, M. J. P., Malcolm, A. J., Mawson, M. H., Staniforth, A., White, A. A., and Wood, N.: A new dynamical core for the Met Office's global and regional modelling of the atmosphere, Quart. J. Roy. Meteor. Soc., 131, 1759–1782, doi:10.1256/qj.04.101, 2005.

Dee, D. P. and Uppala, S.: Variational bias correction of satellite radiance data in the ERA-Interim reanalysis. Q. J. R. Meteor~~ol~~. Soc., 135: 1830-1841, doi: 10.1002/qj.493, 2009.

Dee, D. P., E. Källén, A. J. Simmons, and L. Haimberger: Comments on "Reanalyses suitable for characterizing long-term trends." Bull. Amer. Meteor. Soc., 92, 65–70, doi:10.1175/2010BAMS3070.1, 2011.

Dee, D. P., Uppala, S. M., Simmons, A. J., Berrisford, P., Poli, P., Kobayashi, S., Andrae, U., Balmaseda, M. A., Balsamo, G., Bauer, P., Bechtold, P., Beljaars, A. C. M., van de Berg, L., Bidlot, J., Bormann, N., Delsol. C., Dragani, R., Fuentes, M., Geer, A. J., Haimberger, L., Healy, S. B., Hersbach, H., Holm, E. V., Isaksen, L., Kallberg, P., Kohler, M,, Matricardi, M., McNally, A. P., Monge-Sanz, B. M., Morcrette, J. J., Park, B. K., Peubey, C., de Rosnay, P., Tavolato, C., Thepaut, J. N., Vitart, F.: The Era-Interim reanalysis: Configuration and performance of the data assimilation system, Q. J. R. Meteor. Soc. 137: 553–597, doi: 10.1002/qj.828, 2011.

~~Dee, D. P. and Uppala, S.: Variational bias correction of satellite radiance data in the ERA-Interim reanalysis. Q.J.R. Meteorol. Soc., 135: 1830-1841, doi: 10.1002/qj.493, 2009.~~

Dee, D. P., Balmaseda, M., Balsamo, G., Engelen, R., Simmons, A. J., and Thepaut, J.-N.: Towards a consistent reanalysis of the climate system, B. Am. Meteorol. Soc., 95, 1235–1248, doi:10.1175/BAMS-D-13-00043.1, 2014.

Dharssi, I., Steinle, P., and Candy, B.: Towards a Kalman filter based land surface data assimilation scheme for ACCESS, Bureau of Meteorology CAWCR Technical Report No. 54, http://www.cawcr.gov.au/technical-reports/CTR_054.pdf, 2012.

Dharssi, I., Steinle, P., and Fernon, J.: Improved numerical weather predictions by using optimised urban model parameter values and satellite derived tree heights. In Weber, T., McPhee, M.J. and Anderssen, R.S. (eds) MODSIM2015, 21st International Congress on Modelling and Simulation. Modelling and Simulation Society of Australia and New Zealand, December 2015, pp. 1161–1167. ISBN: 978-0-9872143-5-5. https://www.mssanz.org.au/modsim2015/M4/dharssi.pdf, 2015.

Dharssi, I., and Vinodkumar: JASMIN: A prototype high resolution soil moisture analysis system for Australia, Bureau of Meteorology Report No. 026, http://www.bom.gov.au/research/publications/researchreports/BRR-026.pdf, 2017.

Dickinson, R.E., Errico, R.M., Giorgi, F., and Bates, G. T.: A regional climate model for the western United States, 15: 383-422, doi: 10.1007/BF00240465, 1989.

Donlon, C. J., M. Martin, J. D. Stark, J. Roberts-Jones, E. Fiedler, and W. Wimmer: The Operational Sea Surface Temperature and Sea Ice analysis (OSTIA) system, Rem. Sens. Environ., 116, 140–158, doi: 10.1016/j.rse.2010.10.017, 2012.

Ebert, E.E., J.E. Janowiak, and C. Kidd: Comparison of near-real-time precipitation estimates from satellite observations and numerical models. Bull. Amer. Meteor. Soc., 88, 47–64, doi: 10.1175/BAMS-88-1-47, 2007.

Ebita, A., Kobayashi, S., Ota, Y., Moriya, M., Kumabe, R., Onogi, K., Harada, Y., Yasui, S., Miyaoka, K., Takahashi, K., Kamahori, H., Kobayashi, C., Endo, H., Soma, M., Oikawa, Y., and Ishimizu, T.: The Japanese 55-year reanalysis JRA-55: An interim report, SOLA, 7, 149–152, doi: 10.2151/sola.2011-038, 2011.

Edwards, J. M. and Slingo, A.: Studies with a flexible new radiation code. I: Choosing a configuration for a large-scale model, Quart. J. Roy. Meteorol. Soc., 122, 689–719, doi:10.1002/qj.49712253107, 1996.

Evans, J. P., and McCabe, M. F.: Effect of model resolution on a regional climate model simulation over southeast Australia. Clim. Res., 56,131–145, doi: 10.3354/cr01151, 2013.

Fall, S., Niyogi, D., Gluhovsky, A., Pielke Sr, R. A., Kalnay, E., and Rochon, G.: Impacts of land use land cover on temperature trends over the continental United States: assessment using the North American Regional Reanalysis. Int. J. Climatol., 30, 1980-1993, doi: 10.1002/joc.1996, 2010.

Fowler, H. J., Blenkinshop, S., and Tebaldi, C.: Linking climate change modelling to impacts studies: recent advances in downscaling techniques for hydrological modeling. Int. J. Climatol. 27, 1547–1578, doi: 10.1002/joc.1556, 2007.

Frank, C. W., Wahl, S., Keller, J. D., Pospichal, B., Hense, A., and Crewell, S.: Bias correction of a novel European reanalysis data set for solar energy applications. Solar Energy, 164, 12-24, doi: 10.1016/j.solener.2018.02.012, 2018.

Franklin, C. N., Z. Sun, D. Bi, M. Dix, H. Yan, and A. Bodas-Salcedo: Evaluation of clouds in ACCESS using the satellite simulator package COSP: Global, seasonal, and regional cloud properties, J. Geophys. Res. Atmos., 118, 732–748, doi: 10.1029/2012JD018469, 2013.

Gauthier, P., and Thépaut, J.-N.: Impact of the digital filter as a weak constraint in the preoperational 4DVar assimilation system of Météo-France." Mon. Wea. Rev., 129, 2089-2102, doi: 10.1175/1520-0493(2001)129<2089:IOTDFA>2.0.CO;2, 2001.

Gelaro, R., W. McCarty, M. J. Suárez, R. Todling, A. Molod, L. Takacs, C. A. Randles, A. Darmenov, M. G. Bosilovich, R. Reichle, K. Wargan, L. Coy, R. Cullather, C. Draper, S. Akella, V. Buchard, A. Conaty, A.M. da Silva, W. Gu, G. Kim, R. Koster, R. Lucchesi, D. Merkova, J. E. Nielsen, G. Partyka, S. Pawson, W. Putman, M. Rienecker, S. D. Schubert, M. Sienkiewicz, and B. Zhao: The Modern-Era Retrospective Analysis for Research and Applications, Version 2 (MERRA-2), J. Clim., 30, 5419–5454, doi: 10.1175/JCLI-D-16-0758.1, 2017.

Gregory, D., and P. R. Rowntree: A mass flux convection scheme with representation of cloud ensemble characteristics and stability-dependent closure, Mon. Weath. Rev., 118, 1483–1506, doi: 10.1175/1520-0493(1990)118<1483:AMFCSW>2.0.CO;2, 1990.

Harris, B. A. and Kelly, G.: A satellite radiance-bias correction scheme for data assimilation. Q.J.R. Meteorol. Soc., 127: 1453-1468. doi:10.1002/qj.49712757418, 2001.

Hartmann, D. L., Klein Tank, A. M. G., Rusticucci, M., Alexander, L. V., Brönnimann, S., Charabi, Y., Dentener, F. J., Dlugokencky, E. J., Easterling, D. R., Kaplan, A., Soden, B. J., Thorne, P. W., Wild, M., and Zhai, P. M.: Observations: Atmosphere and Surface, in: Climate Change 2013: The Physical Science Basis. Contribution of Working Group I to the Fifth Assessment Report of the Intergovernmental Panel on Climate Change. Cambridge University Press, Cambridge, United Kingdom and New York, NY, USA, 2013.

Glahn, H. R., and D. A. Lowry: The use of model output statistics (MOS) in objective weather forecasting. J. Appl. Meteor., 11, 1203–1211, doi:10.1175/1520-0450(1972)011,1203:TUOMOS.2.0.CO;2, 1972.

Gustafson Jr., W. I., P.-L. Ma, and B. Singh: Precipitation characteristics of CAM5 physics at mesoscale resolution during MC3E and the impact of convective timescale choice, J. Adv. Model. Earth Syst., 6, 1271–1287, doi:10.1002/ 2014MS000334, 2014.

Hersbach, H., and Dee, D.: ERA5 reanalysis is in production, ECMWF Newsletter No. 147, 7, accessed online https://www.ecmwf.int/sites/default/files/elibrary/2016/16299-newsletter-no147-spring-2016.pdf, 2016.

Holt, E., and Wang, J.: Trends in wind speed at wind turbine height of 80 m over the contiguous United States using the North American Regional Reanalysis (NARR), J. Appl. Meteor. Climatol., 51, 2188–2202, doi: 10.1175/JAMC-D-11-0205.1, 2012.

Howard, T., and Clark, P.: Correction and downscaling of NWP wind speed forecasts, Meteorol. Apps., 14, 105-116, doi: 10.1002/met.12, 2007.

Huffman, G. J., Adler, R. F., Bolvin, D. T., Gu, G., Nelkin, E. J., Bowman, K. P., Hong, Y., Stocker, E. F., and Wolff, D. B.: The TRMM multisatellite precipitation analysis (TMPA): Quasi-global, multiyear, combined-sensor precipitation estimates at fine scales, J. Hydrometeor., 8, 38–54, doi: 10.1175/JHM560.1, 2006.

Ingleby, N. B.: The statistical structure of forecast errors and its representation in The Met. Office Global 3-D variational data assimilation scheme. Q. J. R. Meteor. Soc. 127: 209-231, doi: 10.1002/qj.49712757112, 2001.

Jakob, D., Su, C.-H., Eizenberg, N., Kociuba, G., Steinle, P., Fox-Hughes, P., and Bettio, L.: An atmospheric high-resolution regional reanalysis for Australia, Bull. Aus. Meteor. Oceanog. Soc., 30, 16-23, 2017.

Jermey, P. M., and Renshaw, R. J.: Precipitation representation over a two-year period in regional reanalysis, Q. J. R. Meteorol. Soc., 142, 1300–1310, doi: 10.1002/qj.2733, 2016.

Jones, D. A., Wang, W., and Fawcett, R.: High-quality spatial climate data-sets for Australia, Aust. Meteorol. Oceanogr. J., 58, 233–248, 2009.

Kallberg, P.: Forecast drift in ERA-Interim. ERA report series 10, accessed online https://www.ecmwf.int/sites/default/files/elibrary/2011/10381-forecast-drift-era-interim.pdf, 2011.

Kalnay, E., M. Kanamitsu, R. Kistler, W. Collins, D. Deaven, L. Gandin, M. Iredell, S. Saha, G. White, J. Woollen, Y. Zhu, M. Chelliah, W. Ebisuzaki, W. Higgins, J. Janowiak, K.C. Mo, C. Ropelewski, J. Wang, A. Leetmaa, R. Reynolds, R. Jenne, and D. Joseph: The NCEP/NCAR 40-Year Reanalysis Project. Bull. Amer. Meteor. Soc., 77, 437–472, doi: 10.1175/1520-0477(1996)077<0437:TNYRP>2.0.CO;2, 1996.

Le Marshall, J., Xiao, Y., Norman, R., Zhang, K., Rea, A., Cucurull, L., Seecamp, R., Steinle, P., Puri, K., and Le, T.: The beneficial impact of radio occultation observations on Australian region forecasts, Aust. Meteorol. Oceanogr. J., 60:121–125, 2010.

Le Marshall, J., R. Seecamp, Y. Xiao, P. Gregory, J. Jung, P. Stienle, T. Skinner, C. Tingwell, and T. Le: The Operational Generation of Continuous Winds in the Australian Region and Their Assimilation with 4DVar. Wea. Forecasting, 28, 504–514, doi: 10.1175/WAF-D-12-00018.1, 2013.

Lean, H. W., Clark, P. A., Dixon, M., Roberts, N. M., Fitch, A., Forbes, R., and Halliwell, C.: Characteristics of high-resolution versions of the Met Office Unified Model for forecasting convection over the United Kingdom, Mon. Weath. Rev., 136, 3408–3424, doi: 10.1175/2008MWR2332.1, 2008.

Lock, A. P., Brown, A. R., Bush, M. R., Martin, G. M., and Smith, R. N. B.: A new boundary layer mixing scheme. Part I: Scheme description and single-column model tests, Mon. Weather Rev., 128, 3187–3199, doi:10.1175/1520-0493(2000)128<3187:ANBLMS>2.0.CO;2, 2000.

Lorenc, A. C., and Hammon, O.: Objective quality control of observations using Bayesian methods. Theory, and a practical implementation. Q. J. Roy. Meteor. Soc., 114, 515-543, doi: 10.1002/qj.49711448012, 1988.

Lorenc, A. C.: Modelling of error covariances by 4D-Var data assimilation, Q. J. Roy. Meteor. Soc., 129, 3167–3182, doi: 10.1256/qj.02.131, 2003.

Lorenc, A. C., and Payne, T. J.: 4D-Var and the butterfly Effect: Statistical four-dimensional data assimilation for a wide range of scales, Q. J. Roy. Meteorol. Soc., 133, 607–614, doi: 10.1002/qj.36, 2007.

Loveland, T. R., B. C. Reed, J. F. Brown, D. O. Ohlen, Z. Zhu, L. Yang, and J. W. Merchant: Development of a global land cover characteristics database and IGBP DISCover from 1 km AVHRR data. Int. J. Rem. Sens., 21, 1303–1330, doi: 10.1080/014311600210191, 2000.

Ma, Y., Zhou, X., Bi, D., Sun, Z., and Hirst, A. C.: Improved air-sea flux algorithms in an ocean-atmosphere coupled model for simulation of global ocean SST and its tropical pacific variability, Clim. Dyn., 44, 1473–1485, doi: 10.1007/s00382-014-2281-7, 2015.

Mahmood, S., Davie, J., Jermey, P., Renshaw, R., George, J. P., Rajagopal, E. N., and Rani, S. I.: Indian monsoon data assimilation and analysis regional reanalysis: Configuration and performance, Atmos. Sci. Lett., 19, doi: 10.1002/asl.808, 2018.

Malloy, J.W., D.S. Krahenbuhl, C.E. Bush, R.C. Balling, M.M. Santoro, J.R. White, R.C. Elder, M.B. Pace, and R.S. Cerveny: A surface wind extremes (“wind lulls” and “wind blows”) climatology for central North America and adjoining oceans (1979–2012). J. Appl. Meteor. Climatol., 54, 643–657, doi: 10.1175/JAMC-D-14-0009.1, 2015.

Martynov, A., Laprise, R., Sushama, L., Winger, K., Separovic, L., and Dugas, B.: Reanalysis-driven climate simulation over CORDEX North America domain using the Canadian Regional Climate Model, version 5: model performance evaluation. Clim. Dyn., 41, 2973-3005, doi: 10.1007/s00382-013-1778-9, 2013.

Masunaga, R., H. Nakamura, T. Miyasaka, K. Nishii, and Y. Tanimoto: Separation of climatological imprints of the Kuroshio Extension and Oyashio fronts on the wintertime atmospheric boundary layer: Their sensitivity to SST resolution prescribed for atmospheric reanalysis. J. Climate, 28, 1764−1787, doi: 10.1175/JCLI-D-14-00314.1, 2015.

Masunaga, R., Nakamura, H., Kamahori, H., Onogi, K., and Okajima, S.: JRA-55CHS: An atmospheric reanalysis produced with high-resolution SST, SOLA, 14, 6-13, doi: 10.2151/sola.2018-002, 2018.

Matthews, A. J., Pickup, G., Peatman, S.C., Clews, P., and Martin, J.: The effect of the Madden-Julian Oscillation on station rainfall and riverlevel in the Fly River System, Papua New Guinea, J. Geophys. Res. Atmos., 118, 10926–10935, doi:10.1002/jgrd.50865, 2013.

Mesinger, F., G. DiMego, E. Kalnay, K. Mitchell, P.C. Shafran, W. Ebisuzaki, D. Jović, J. Woollen, E. Rogers, E.H. Berbery, M.B. Ek, Y. Fan, R. Grumbine, W. Higgins, H. Li, Y. Lin, G. Manikin, D. Parrish, and W. Shi: North American Regional Reanalysis, Bull. Amer. Meteor. Soc., 87, 343–360, doi: 10.1175/BAMS-87-3-343, 2006.

Moore, R. J.: The PDM rainfall-runoff model. Hydrol. Earth Syst. Sci., 11: 483-499, doi: 10.5194/hess-11-483-2007, 2007.

Puri, K., G. Dietachmayer, P. Steinle, M. Dix, L. Rikus, L. Logan, M. Naughton, C. Tingwell, Y. Xiao, V. Barras, I. Bermous, R. Bowen, L. Deschamps, C. Franklin, J. Fraser, T. Glowacki, B. Harris, J. Lee, T. Le, G. Roff, A. Sulaiman, H. Sims, X. Sun, Z. Sun, H. Zhu, M. Chattopadhyay and C. Engel, Implementation of the initial ACCESS numerical weather prediction system. Aust. Meteorol. Oceanogr. J., 63, 265-284, 2013.

Radic, V., and Clarke, G. K. C.: Evaluation of IPCC models’ performance in simulating late-twentieth-century climatologies and weather Patterns over North America. J. Climate, 24, 5257–5274, doi: 10.1175/JCLI-D-11-00011.1, 2011.

Ramella Pralungo, L., Haimberger, L., Stickler, A., and Brönnimann, S.: A global radiosonde and tracked balloon archive on 16 pressure levels (GRASP) back to 1905 – Part 1: Merging and interpolation to 00:00 and 12:00 GMT, Earth Syst. Sci. Data, 6, 185-200, doi: 10.5194/essd-6-185-2014, 2014.

Ramella Pralungo, L., and Haimberger, L.: A "Global Radiosonde and tracked-balloon Archive on Sixteen Pressure levels" (GRASP) going back to 1905 – Part 2: homogeneity adjustments for pilot balloon and radiosonde wind data, Earth Syst. Sci. Data, 6, 297-316, doi: 10.5194/essd-6-297-2014, 2014.

Rawlins, F., Ballard, S. P., Bovis, K. J., Clayton, A. M., Li, D., Inverarity, G. W., Lorenc, A. C., and Payne, T. J.: The Met Office global 4-dimensional data assimilation system. Q. J. Roy. Met. Soc., 133, 347–362, doi: 10.1002/qj.32, 2007.

Randall D. A., et. al., Climate models and their evaluation. In: climate change 2007: The physical science basis. Contribution of working group I to the fourth assessment report of the intergovernmental panel on climate change. In: Solomon, S., Qin, D., Manning, M., Chen, Z., Marquis, M., Averyt, K. B., Tignor, M., and Miller, H. L. (eds.) Cambridge University Press, Cambridge and New York, NY, 2007.

Renshaw, R., Jermey, P., Barker, D., Maycock, A., and Oxley, S.: EURO4M regional reanalysis system. Forecasting Research Technical Report No. 583, ~~accessed online: h~~https://www.metoffice.gov.uk/binaries/content/assets/mohippo/pdf/o/4/frtr583.pdf (last access: 13 February 2018), 2013.

Ridal, M., Olsson, E., Unden, P., Zimmermann, K., and Ohlsson, A.: HARMONIE reanalysis report of results and dataset, UERRA Project Deliverable D2.7, http://www.uerra.eu/ (last access: 13 February 2018), 2017.

Roberts-Jones, J., E.K. Fiedler, and M.J. Martin: Daily, global, high-resolution SST and sea ice reanalysis for 1985–2007 Using the OSTIA system, J. Clim., 25, 6215–6232, doi: 10.1175/JCLI-D-11-00648.1, 2012.

Rose, S., and Apt, J.: Quantifying sources of uncertainty in reanalysis derived wind speed, Renewable Energy, 94, 157-165, doi: 10.1016/j.renene.2016.03.028, 2016.

Ruiz-Barradas, A. and Nigam, S.: IPCC's twentieth-century climate simulations: Varied representations of North American hydroclimate variability. J. Clim., 19, 4041–4058, doi: 10.1175/JCLI3809.1, 2006.

Sapiano, M. R. P., and Arkin, P. A.: An intercomparison and validation of high-resolution satellite precipitation estimates with 3-hourly gauge data, J. Hydrometeor., 10, 149-166, doi: 10.1175/2008JHM1052.1, 2009.

Scinocca, J. F., and McFarlane, N. A.: The variability of modeled tropical precipitation, J. Atmos. Sci., 61, 1993–2015, 2004.

Sheridan, P., Smith, S., Brown, A., and Vosper, S.: A simple height-based correction for temperature downscaling in complex terrain, Meteor. App., 17, 329-339, doi: 10.1002/met.177, 2010.

Smith, I., A. Moise, K. Inape, B. Murphy, R. Colman, S. Power, and C. Chung: ENSO-related rainfall changes over the New Guinea region, J. Geophys. Res. Atmos., 118, 10,665–10,675, doi:10.1002/jgrd.50818, 2013.

Simard, M., N. Pinto, J. B. Fisher, and A. Baccini: Mapping forest canopy height globally with spaceborne lidar. J. Geophys. Res.: Biogeosci., 116, G04021, doi:10.1029/2011JG001708, 2011.

Thorne, P. W., and R. S. Vose: Reanalyses suitable for characterizing long-term trends. Bull. Amer. Meteor. Soc., 91, 353–361, doi:10.1175/2009BAMS2858.1, 2010.

Walters, D., Boutle, I., Brooks, M., Melvin, T., Stratton, R., Vosper, S., et al.: The Met Office Unified Model Global Atmosphere 6.0/6.1 and JULES Global Land 6.0/6.1 configurations. Geosci. Model. Dev., 10, 1487–1520, doi: 10.5194/gmd-10-1487-2017, 2017a.

Walters, D., Baran, A., Boutle, I., Brooks, M., Earnshaw, P., Edwards, J., et al.: The Met Office Unified Model Global Atmosphere 7.0/7.1 and JULES Global Land 7.0 configurations. Geosci Model Dev. Discuss., doi: 10.5194/gmd-2017-291, 2017b.

Wang, Z., Siems, S. T., Belusic, D., Manton, M. J., and Huang, Y.: A climatology of the precipitation over the Southern Ocean as observed at Macquarie Island. J. Appl. Meteorol. Climatol., 54, 2321-2337, doi: 10.1175/JAMC-D-14-0211.1, 2015.

Williamson, D. L.: The effect of time steps and time-scales on parametrization suites, Q. J. R. Meteorol. Soc., 139, 548–560, doi:10.1002/qj.1992, 2013.

Wilson, D. R. and Ballard, S. P.: A microphysically based precipitation scheme for the UK Meteorological Office Unified Model, Q. J. R. Meteorol. Soc., 125, 1607–1636, doi:10.1002/qj.49712555707, 1999.

Wood, N., Staniforth, A., White, A., Allen, T., Diamantakis, M., Gross, M., Melvin, T., Smith, C., Vosper, S., Zerroukat, M., and Thuburn, J.: An inherently mass-conserving semi-implicit semi-Lagrangian discretization of the deep-atmosphere global non-hydrostatic equations, Q. J. R. Meteorol. Soc., 140, 1505–1520, doi:10.1002/qj.2235, 2014.

Ziese, M., Rauthe-Schöch, A., Becker, A., Finger, P., Meyer-Christoffer, A, and Schneider, U: GPCC full data daily version.2018 at 1.0°: Daily land-surface precipitation from rain-gauges built on GTS-based and historic data. doi: 10.5676/DWD_GPCC/FD_D_V2018_100, 2018.

Zhao, M., Zhang, H-Q., and Dharssi, I.: Impact of land-surface initialization on ACCESS-S1 and comparison with POAMA. Bureau of Meteorology Research Report No. 023, Accessed online: http://www.bom.gov.au/research/publications/researchreports/BRR-023.pdf, 2017.

Zhu, H., and Dietachmayer, G.: Improving ACCESS-C convection settings, Bureau Research Report No. 008, Accessed online: http://www.bom.gov.au/research/publications/researchreports/BRR-008.pdf, 2015.

Zick, S. E., and Matyas, C. J.: Tropical cyclones in the North American Regional Reanalysis: An assessment of spatial biases in location, intensity, and structure, J. Geophys. Res.: Atmos., 120, 1651-1669, doi: 10.1002/2014JD022417, 2015.

Figures

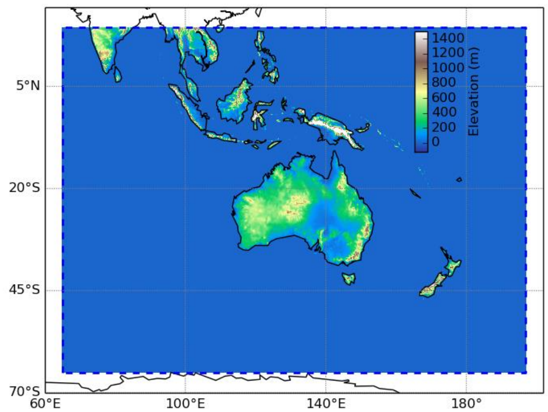

Figure 1~~1~~ BARRA-R domain enclosed by the dashed box. Blue shading shows the model orography.

Formatted: Check spelling and grammar

Formatted: Font: (Default) Times New Roman, Font color: Auto

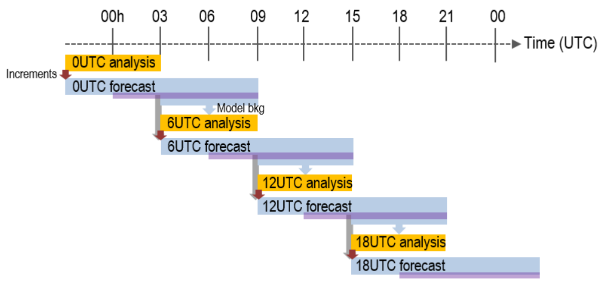

Figure 22 Cycling setup of BARRA-R at base time t_0 = 0, 6, 12, and 18 UTC. Each UM forecast is initialized at t_0-3h by the previous forecast (grey arrows) with increments from current analysis (red arrows). The purple bars indicate the time steps of the model states that have been archived.

Formatted: Check spelling and grammar

Formatted: Font: (Default) Times New Roman, Font color: Auto

Formatted: Font: (Default) Times New Roman, Font color: Auto, Not Superscript/ Subscript

Formatted: Font: (Default) Times New Roman, Font color: Auto

Formatted: Font: (Default) Times New Roman, Font color: Auto, Not Superscript/ Subscript

Formatted: Font: (Default) Times New Roman, Font color: Auto

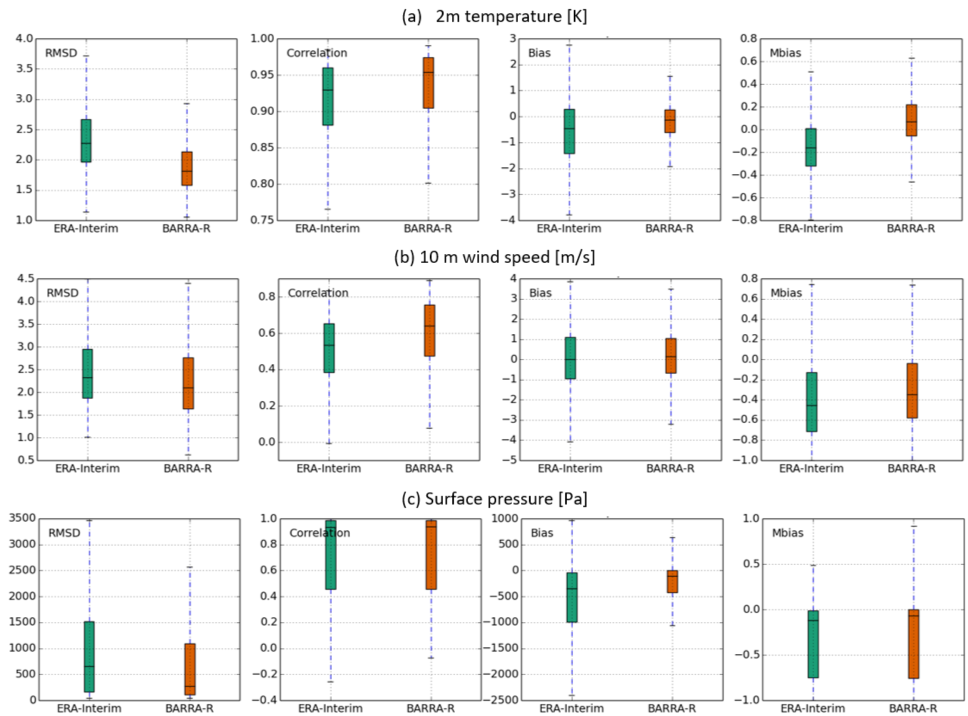
(a) 2m temperature [K]
RMSD
Correlation
Bias
Mbias
ERA-Interim
BARRA-R
(b) 10 m wind speed [m/s]
RMSD
Correlation
Bias
Mbias
ERA-Interim
BARRA-R
(c) Surface pressure [Pa]
RMSD
Correlation
Bias
Mbias
ERA-Interim
BARRA-R

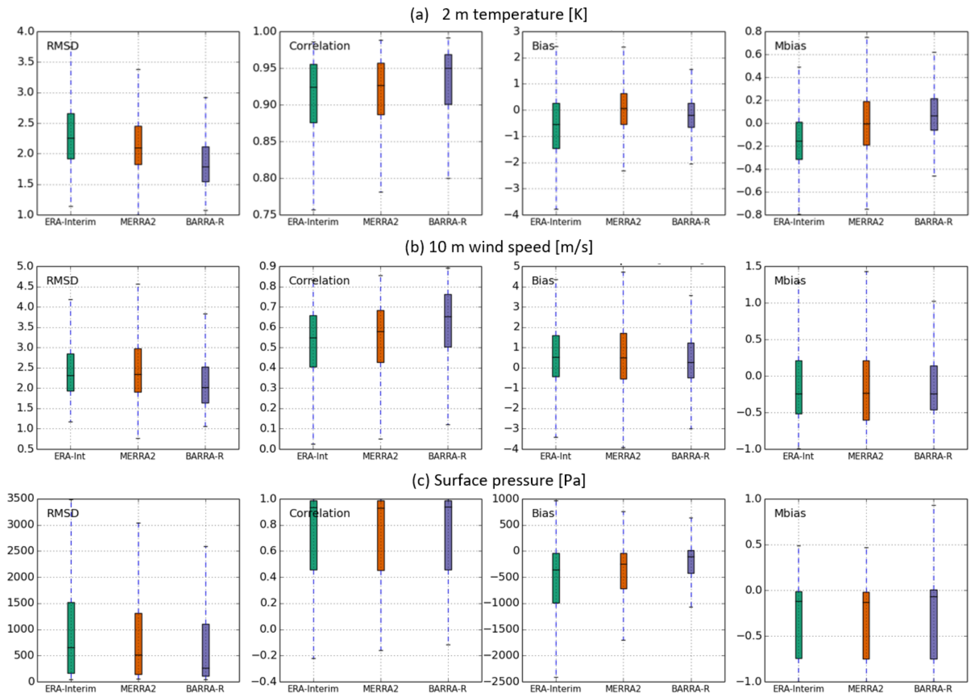

Figure 3 Boxplots showing the distribution of ERA-Interim, MERRA-2, and BARRA-R ~~and ERA-Interim t_0+6h forecast~~evaluation scores for (a) 2 m temperature, (b) 10 m wind speed, and (c) surface pressure over all stations in the BARRA-R domain. The scores are calculated on model forecasts valid between t_0+5h and t_0+7h against observations during 2007-2016. Individual boxes ~~extend~~ show the interquartile range of the scores~~from first to third quartile~~, ~~.~~ ~~Medians~~ medians are marked in each box and 'whiskers' cover the 5-95% percentile range.

Formatted: Subscript

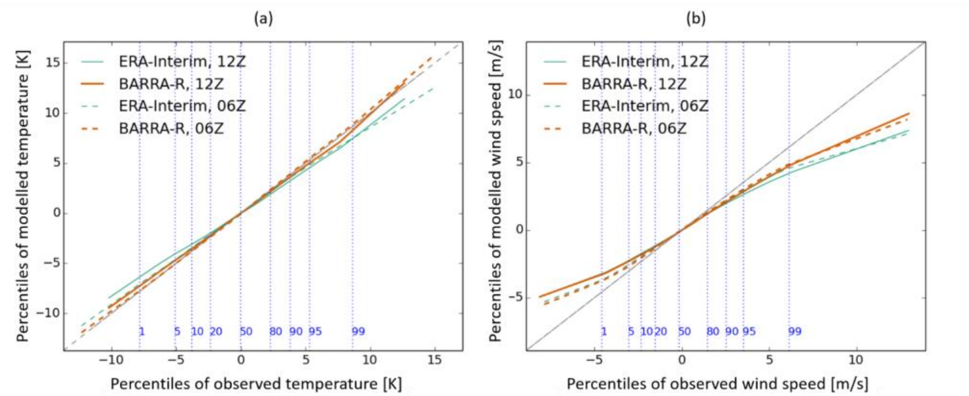

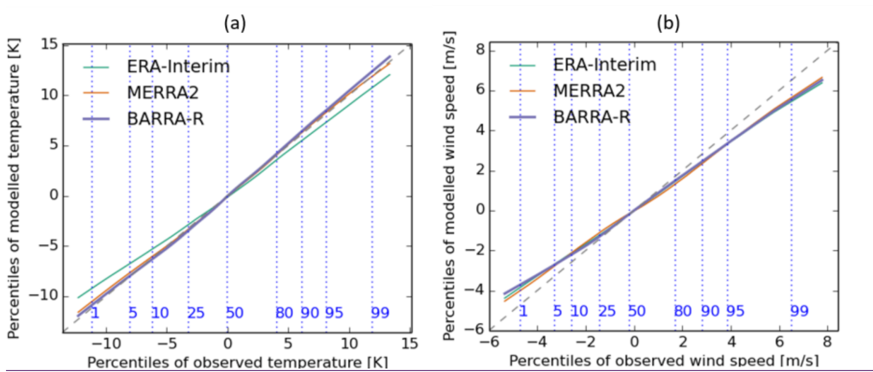

Figure 4 Comparisons of percentile values between observations and reanalyses for (a) 2 m temperature, and (b) 10 m wind speed during 2010-2013. The values from 0.05% to 99.95% percentiles are calculated using values derived from monthly means. The vertical blue dashed lines indicate the corresponding percentiles of the observations.

Formatted: Centered

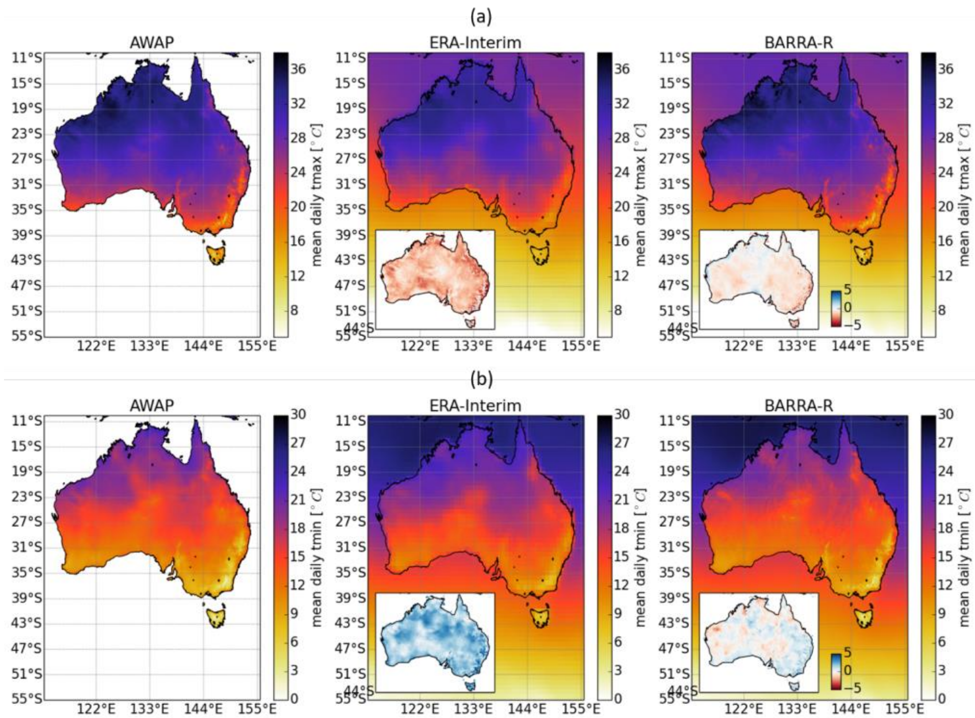
(a)
AWAP
ERA-Interim
BARRA-R
mean daily tmax [°C]
(b)
AWAP
ERA-Interim
BARRA-R
mean daily tmin [°C]

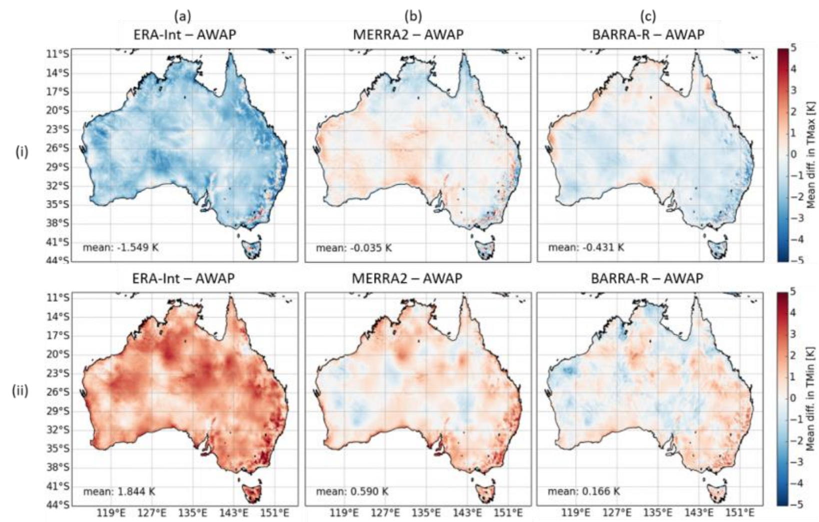

Figure 5 Mean differences in (row i) ~~Mean~~ **daily** ~~minimum~~ maximum (TMax) ~~(top row)~~ **and** (ii) ~~maximum~~ minimum~~(bottom row)~~ ~~screen~~ 2 m **temperature** [K] for 2007-2016, between (column a) ERA-Interim and AWAP, (b) MERRA-2 and AWAP, and (c) BARRA-R and AWAP. The spatial means of the differences ~~from AWAP, ERA-Interim and BARRA-R. The insets show differences when subtracting AWAP statistic from the reanalyses.~~ are reported in text.

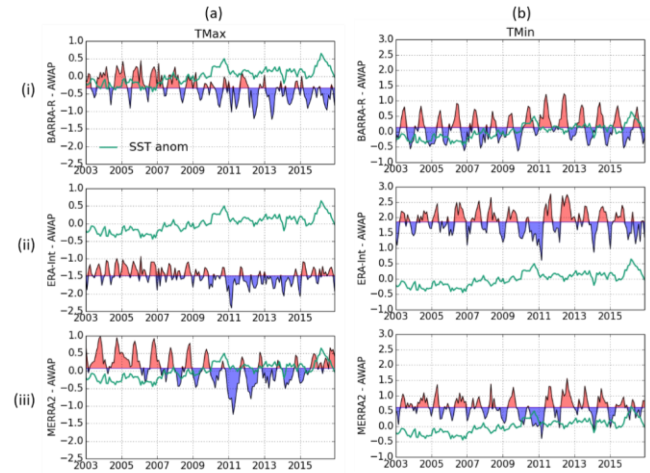

Figure 6 Monthly mean differences in daily (column a) maximum (TMax) and (b) minimum (TMin) 2 m temperature [K] averaged over Australia, between (row i) BARRA-R and AWAP, (ii) ERA-Interim and AWAP, and (iii) MERRA-2 and AWAP. Black curves are shaded around the 14-year means. Green curves plot the monthly anomalies, from 2003-2016 monthly averages, of the OSTIA sea surface temperature averaged over 46-4° S and 94-174°E.

Formatted: Centered

Formatted: Caption

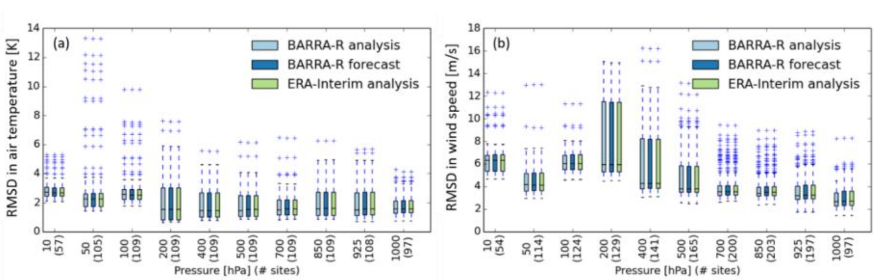

Figure 7~~6~~ Boxplots showing the RMSD ~~RMSD~~ distribution of BARRA-R t_0+6 forecast and t_0 analysis, and ERA-Interim analysis for (a) temperature and (b) wind speed at over multiple sites in the BARRA-R domain. RMSD is calculated for temperature and wind speed at pressure levels 10, 50, 100, 200, 400, 500, 700, 850, 925 and 1000 hPa against pilot balloon and radiosonde observations at 0 and 12 UTC. The numbers of sites are indicated in the brackets.

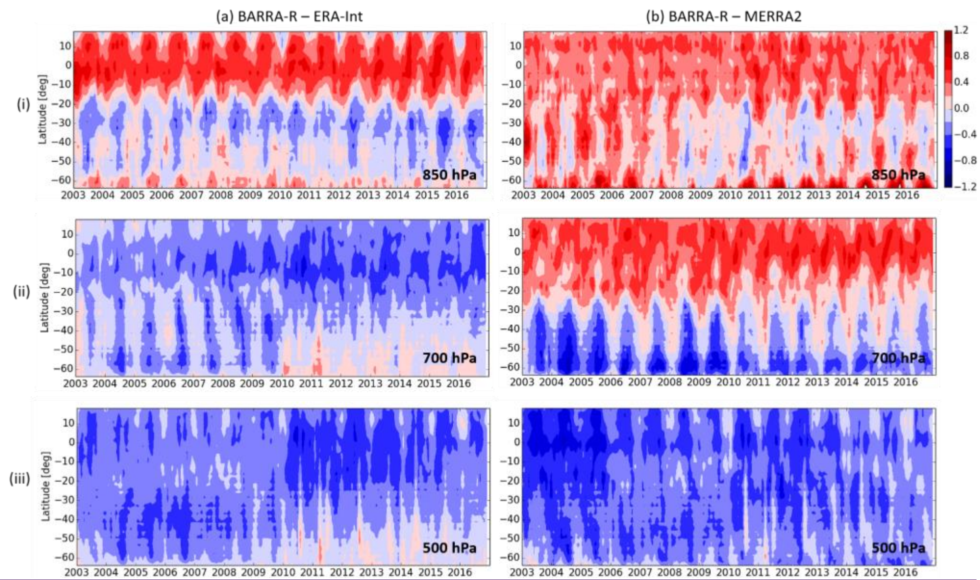

Figure 8 Hovmöller plots of the monthly difference in zonal mean air temperature [K] at 0 UTC and three pressure levels (row i) 850, (ii) 700, and (iii) 500 hPa, between (column a) BARRA-R and ERA-Interim, and (b) BARRA-R and MERRA-2.

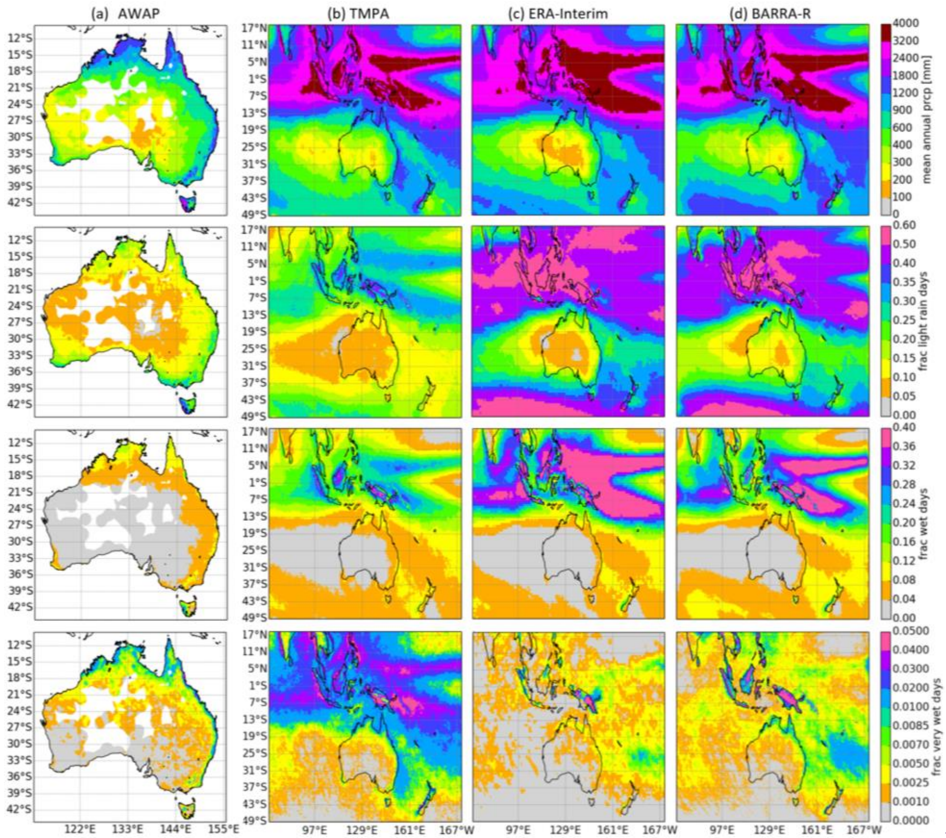
(a) AWAP
(b) TMPA
(c) ERA-Interim
(d) BARRA-R
mean annual prcp [mm]
frac light rain days
frac wet days
frac very wet days
122°E
133°E
144°E
155°E
97°E
129°E
161°E
167°W

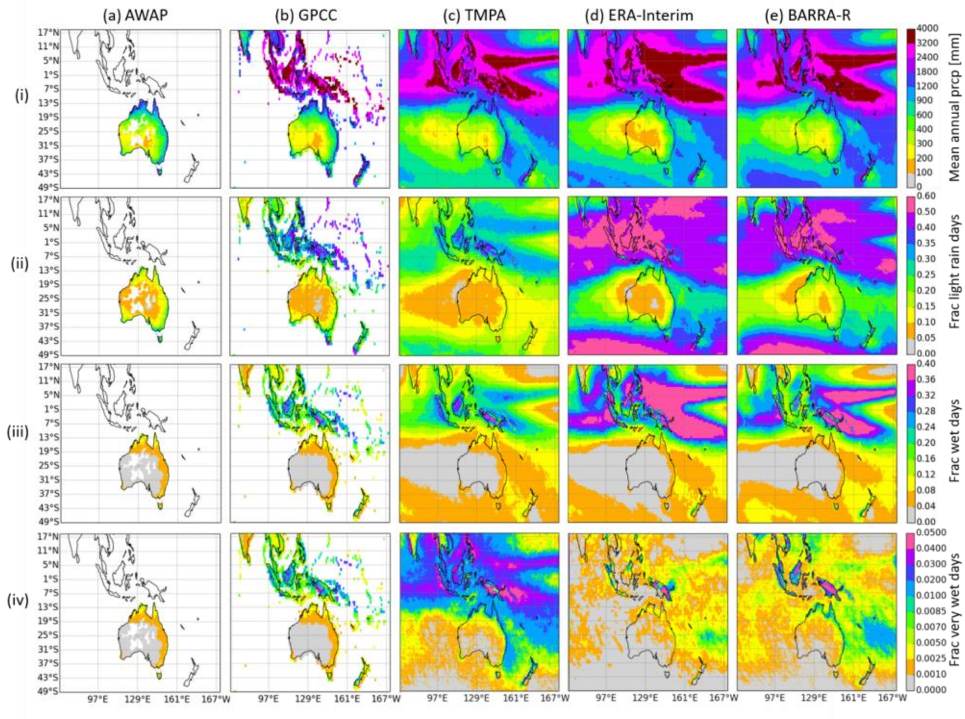

Figure 9~~7~~ (row i) Mean annual precipitation [mm] ~~(top row)~~, and (ii) fractions of light rain days with 1-10 mm precipitation ~~(second row)~~, (iii) heavy precipitation days with 10-50 mm ~~(third row)~~ and (iv) very heavy precipitation days with > 50 mm ~~(bottom)~~, ~~from~~ over 2007~~- to~~ 2016 from (column a) AWAP ~~(first column)~~, (b) GPCC, (c) TMPA ~~(second column)~~, (d) ERA-Interim ~~(third column)~~, and (e) BARRA-R ~~(last column)~~. Regions with more than 10% missing values in AWAP are masked. Close ups of the plots over Australia are provided in the Supplementary Material.

Formatted: Normal

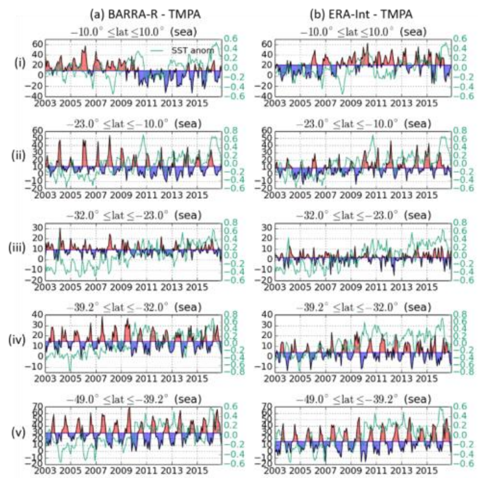
(a) BARRA-R - TMPA
(b) ERA-Int - TMPA
$-10.0^\circ \leq$lat$\leq 10.0^\circ$ (sea)
SST anom
(i)
$-23.0^\circ \leq$lat$\leq -10.0^\circ$ (sea)
(ii)
$-32.0^\circ \leq$lat$\leq -23.0^\circ$ (sea)
(iii)
$-39.2^\circ \leq$lat$\leq -32.0^\circ$ (sea)
(iv)
$-49.0^\circ \leq$lat$\leq -39.2^\circ$ (sea)
(v)
2003 2005 2007 2009 2011 2013 2015

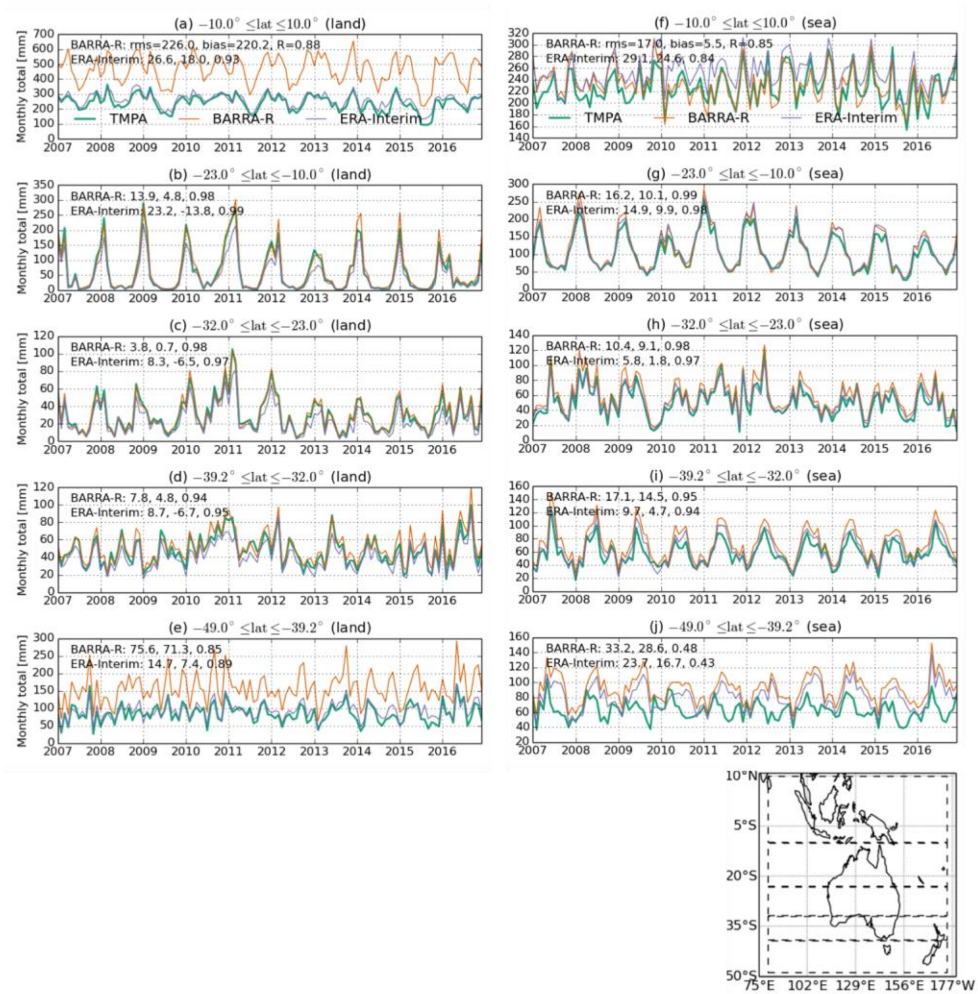

Figure ~~8~~10 Differences in ~~Monthly~~ monthly ~~mean~~ precipitation total [mm] averaged over the ocean in five sub-domains (row i-v), between (column a) BARRA-R and TMPA, and (b) ERA-Interim and TMPA. Black curves are shaded around the 14-year means. Green curves plot the monthly anomalies, from 2003-2016 monthly averages, of the OSTIA sea surface temperature averaged over respective sub-domains.~~land (left) and sea (right), from TMPA, ERA-Interim and BARRA-R, in five sub-domains depicted in the inset. RMSD, bias and correlation are calculated between each reanalysis and TMPA.~~

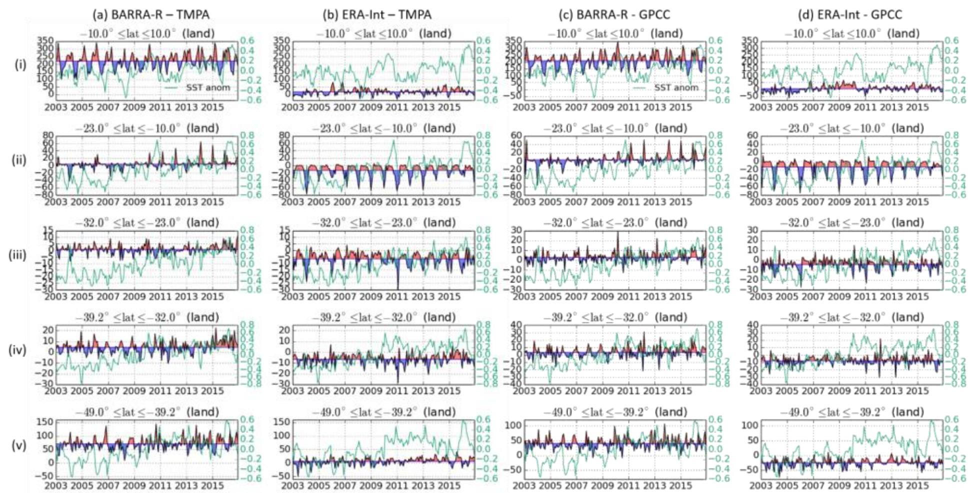

Figure 11 As with ~~Figure 9~~ Figure 108 (column a) and (b), but over land. Additional comparisons are made between (c) BARRA-R and GPCC, and (d) ERA-Interim and GPCC.

Formatted: Centered

Tables

Observations	Variables	Time periods	Sources
Land synoptic observations (LNDSYN)	Surface pressure, temperature, humidity, wind	1978-2018~~7~~	Reanalysis prior to 2003 uses the data from ECMWF archive collected for ERA-Interim and ERA-40.~~.~~ Reanalysis between 2003 and 2009 ~~-~~uses the data from ~~UKMO~~ ECMWF operational archive.~~.~~ Reanalysis from 2017 uses satellite radiance data from the UKMO operational archive. Reanalysis from 2010 also uses satellite data from the Bureau's operational archive. Bureau's archive also provides 10 minute land synoptic data from 2001, METARS between 2000 to 2009, TEMP from 2002 and WINPRO from 2010. New Zealand National Climate Database (CliDB) provides additional LNDSYN data over New Zealand.
Meteorological airfield reports (METARS)			
Ship synoptic observations (SHPSYN)			
Buoy	Surface pressure, temperature, wind		
Radiosondes (TEMP)	Upper-air wind, temperature, humidity	1978-2009	
Wind profilers (WINPRO)			
Wind-only sondes (PILOT)	Upper-air wind	1978-2018~~7~~	
Aircraft Meteorological Data Relay (AMDAR)	Flight-level temperature, wind	1978-2018~~7~~	
Air Report (AIREP)			
Advanced Infrared Sounder (AIRS)	Infrared radiances	2003-2018~~7~~	
Advanced TIROS operational vertical sounder (ATOVS)	HIRS/AMSU radiances	1998-2018~~7~~	
TIROS operational vertical sounder (TOVS)	MSU and HIRS radiances	1979-2002	
Infrared Atmospheric Sounding Interferometer (IASI)	Infrared radiances	2007-2018~~7~~	
ESA Cloud motion winds (ESACMW)	Satellite radiometer-based winds (satwinds): cloud motion winds, AMV	1982-2018~~7~~	
Geostationary Operational Environmental (GOESBUFR)		1995-2018~~7~~	
Meteosat 2nd Generation satellite winds (MSGWINDS)		1982-2018~~7~~	
Japanese Geostationary satellite winds (JMAWINDS)		1987-2018~~7~~	
MODIS winds (MODIS)		2005-2018~~7~~	
SeaWinds	Scatterometer-based winds (scatwinds)	1996-2009	
Advanced Scatterometer (ASCAT)		2007-2018~~7~~	
GPS Radio Occultation (GPSRO)	Bending angle	2001-2018~~7~~	Reanalysis prior to 2010 uses data provided by Radio Occultation Meteorology Satellite Application Facility (ROM SAF) archive, under EUMETSAT. Reanalysis from 2010 uses the data from the Bureau's operational archive.
Australian locally derived satwinds	AMV	2002-2018~~7~~	Bureau of Meteorology operational archive
WindSat	Scatwinds	2015-2018~~7~~	
Advanced Technology Microwave Sounder (ATMS)	Microwave radiances	2014-2018~~7~~	
Cross-track Infrared Sounder (CrIS)	Infrared radiances	2014-2018~~7~~	
Tropical Cyclone track (TCBOGUS)	Central pressure and position	1848-2018~~6~~	The International Best Track Archive for Climate Stewardship (IBTrACS) provides the track data up to 2017. The Australian Tropical Cyclone Database is used for 2018.

Table 1 Observations assimilated in BARRA. Only the period concurrent with the reanalysis period is used. The various data sets were retrieved during the production, and thus the exact periods of each set used may differ.

	~~**O-B**~~		~~**O-A**~~	
~~**Fields**~~	~~**Bias**~~	~~**RMSD**~~	~~**Bias**~~	~~**RMSD**~~
~~Surface temperature (K)~~	~~-0.09~~	~~1.78~~	~~-0.10~~	~~1.61~~
~~Surface pressure (Pa)~~	~~-3.67~~	~~101.69~~	~~-2.08~~	~~68.85~~
~~Surface relative humidity (%)~~	~~0.0~~	~~10.0~~	~~0.00~~	~~8.0~~
~~Surface zonal wind (m/s)~~	~~0.05~~	~~1.97~~	~~-0.01~~	~~1.74~~
~~Surface meridional wind (m/s)~~	~~0.04~~	~~1.94~~	~~0.01~~	~~1.72~~
~~Aircraft potential temperature (K)~~	~~-0.24~~	~~1.34~~	~~-0.17~~	~~1.10~~
~~Aircraft zonal wind (m/s)~~	~~-0.04~~	~~3.05~~	~~-0.03~~	~~2.09~~
~~Aircraft meridional wind (m/s)~~	~~-0.18~~	~~3.06~~	~~-0.07~~	~~2.07~~
~~Sonde temperature at 980 hPa (K)~~	~~-0.15~~	~~1.11~~	~~-0.08~~	~~0.81~~
~~Sonde temperature at 500 hPa (K)~~	~~-0.33~~	~~0.92~~	~~-0.18~~	~~0.60~~
~~Sonde zonal wind at 980 hPa (m/s)~~	~~-0.15~~	~~2.45~~	~~-0.06~~	~~1.45~~
~~Sonde zonal wind at 500 hPa (m/s)~~	~~-0.17~~	~~2.52~~	~~-0.07~~	~~1.41~~
~~Sonde meridional wind at 980 hPa (m/s)~~	~~0.23~~	~~2.34~~	~~0.09~~	~~1.38~~
~~Sonde meridional wind at 500 hPa (m/s)~~	~~0.11~~	~~2.44~~	~~0.03~~	~~1.39~~
~~Satwind zonal wind (m/s)~~	~~0.36~~	~~3.16~~	~~0.27~~	~~2.72~~
~~Satwind meridional wind (m/s)~~	~~0.05~~	~~2.90~~	~~0.01~~	~~2.40~~
~~Scatwind zonal wind (m/s)~~	~~0.06~~	~~1.39~~	~~0.03~~	~~0.95~~
~~Scatwind meridional wind (m/s)~~	~~0.20~~	~~1.78~~	~~-0.02~~	~~1.32~~

Formatted Table

~~**Table 2 - Comparisons of the 10-year mean of the RMSD and bias between the analyses and observations (O-A) and those between the background and observations (O-B), calculated for selected observational types across the BARRA-R domain. Values in green show reduction in the RMSD and the magnitude of the bias by the analyses, otherwise in red.**~~